ARMY RESEARCH LABORATORY

High Resolution
Electro-Optical Aerosol Phase Function Database
PFNDAT2006

by
Richard C. Shirkey
and
David H. Tofsted

ARL-TR-3877 **August 2006**

NOTICES

Disclaimers

The findings in this report are not to be construed as an official Department of the Army position unless so designated by other authorized documents.

Citation of manufacturer's or trade names does not constitute an official endorsement or approval of the use thereof.

Destroy this report when it is no longer needed. Do not return it to the originator.

Army Research Laboratory
White Sands Missile Range, NM 88002-5501

ARL-TR-3877 **August 2006**

High Resolution Electro-Optical Aerosol Phase Function Database PFNDAT2006

Richard C. Shirkey
and
David H. Tofsted
Computational Information Sciences Directorate

REPORT DOCUMENTATION PAGE

Form Approved
OMB No. 0704-0188

1. REPORT DATE *(DD-MM-YYYY)*	2. REPORT TYPE	3. DATES COVERED (From - To)
August 2006	Final	2006

4. TITLE AND SUBTITLE
High Resolution Electro-Optical Aerosol Phase Function Database PFNDAT2006

5a. CONTRACT NUMBER

5b. GRANT NUMBER

5c. PROGRAM ELEMENT NUMBER

6. AUTHOR(S)
Richard C. Shirkey and David H. Tofsted

5d. PROJECT NUMBER

5e. TASK NUMBER

5f. WORK UNIT NUMBER

7. PERFORMING ORGANIZATION NAME(S) AND ADDRESS(ES)
U.S. Army Research Laboratory
Computational and Information Sciences Directorate
Battlefield Environment Division (ATTN: AMSRD-ARL-CI-EE)
White Sands Missile Range, NM 88002-5501

8. PERFORMING ORGANIZATION REPORT NUMBER
ARL-TR-3877

9. SPONSORING/MONITORING AGENCY NAME(S) AND ADDRESS(ES)
U.S. Army Research Laboratory
2800 Powder Mill Road
Adelphi, MD 20783-1145

10. SPONSOR/MONITOR'S ACRONYM(S)

11. SPONSOR/MONITOR'S REPORT NUMBER(S)
ARL-TR-3877

12. DISTRIBUTION/AVAILABILITY STATEMENT
Approved for public release; distribution is unlimited.

13. SUPPLEMENTARY NOTES

14. ABSTRACT

The High Resolution Phase Function Database (PFNDAT) 2006 consists of a series of wavelength dependent phase functions, single scattering albedos, extinction coefficients, and asymmetry parameters for ten naturally occurring and four manmade aerosols along with brief descriptions of the scattering parameters, concentrations, and aerosol size distribution characteristics. The naturally occurring aerosols consist of maritime, urban, rural, tropospheric, fog, rain, snow, and dust aerosols; a wind-lofted desert aerosol; and the Navy Aerosol Model (NAM). The manmade aerosols consist of dust produced from high-explosive munitions, white phosphorus, fog oil, and hexachloroethane smokes. Many of the models are functions of relative humidity (RH), wind speed, and other parameters. The database includes information at wavelengths from 0.20 to 40.0 μm, dependent on the availability of index of refraction data for each scattering species. PFNDAT2006 includes all PFNDAT2005 aerosols at increased angular and wavelength resolution: 153 angles versus the previous 65 angles. Additional information is provided for the NAM, and radiative transfer calculations are presented comparing the new Henyey-Greenstein snow phase function with the traditional Mie generated phase function. We corrected the following errors: the refractive index of white phosphorus at 1.06 μm and 0%RH; all tropospheric aerosol values were calculated at 99% RH; and the snow phase functions were missing at 10.0 μm and had two values for 11.0 μm. Improvements include updated refractive indices for dust and wind-lofted desert aerosols. These and other minor changes have resulted in improved values. All updated values are included in the 65-angle version of PFNDAT2005 on the CD.

15. SUBJECT TERMS
aerosols, scattering, phase function, transmission

16. SECURITY CLASSIFICATION OF:			17. LIMITATION OF ABSTRACT	18. NUMBER OF PAGES	19a. NAME OF RESPONSIBLE PERSON
a. REPORT	b. ABSTRACT	c. THIS PAGE			Richard C. Shirkey
U	U	U	SAR	60	19b. TELEPHONE NUMBER (*Include area code*) (505) 678-5470

Standard Form 298 (Rev. 8/98)
Prescribed by ANSI Std. Z39.18

Contents

List of Figures

List of Tables

Preface

The 2006 edition of the High Resolution Electro-Optical Aerosol Phase Function Database (PFNDAT2006) consists of a series of wavelength dependent phase functions, single scattering albedos, extinction coefficients, and other relevant properties for ten naturally occurring and four manmade aerosols characteristic of the near surface battlespace. These phase functions are useful in simulating the near surface atmospheric propagation conditions for target acquisition and scattering studies where typical scattering species are required. The naturally occurring aerosols consist of maritime, urban, rural, tropospheric, fog, rain, snow, and dust aerosols; a wind-lofted desert aerosol; and the Navy Aerosol Model of the marine boundary layer. The manmade aerosols consist of dust produced from high-explosive munitions, white phosphorus, fog oil, and hexachloroethane smokes. Many of the models are functions of relative humidity, wind speed, and other parameters, resulting in a total of 69 aerosol variations. Users may also create new composite (mixed) aerosols (e.g., rain plus haze) by making linear combinations of aerosol statistics.

The database includes information at wavelengths from 0.20 to 40.0 μm, dependent on the availability of index of refraction data for each scattering species. This report contains brief descriptions of the scattering parameters and the aerosol size distribution characteristics used to generate the phase functions, albedos, extinction coefficients, and asymmetry parameters. This version of PFNDAT includes all 2005 phase functions at an expanded angular resolution. For most aerosols, the wavelength resolution was also expanded. There are now 153 discrete angles ranging from 0° to 180°, which are highly concentrated in the forward peak direction. The increased angular resolution allows for more accurate scattering calculations. PFNDAT2005 now incorporates these more accurate concentrations, number densities, and asymmetry factors although it still maintains the original 65 angular resolution. The 2005 and 2006 phase functions and associated parameters are provided on CD along with a short computer program that may be used to interrogate them.

Executive Summary

In order to acquire targets on the dirty battlefield, we must know how much "signal" is lost as it propagates through the atmosphere from the target to the sensor, and how much "noise" is added back in through atmospheric scattering processes. These effects are often expressed as a loss of target contrast. Calculating this quantity requires information about the atmospheric constituents and how they interact with radiation of various wavelengths passing through the atmosphere. The aerosol Phase Function Database (PFNDAT) is a repository of aerosol scattering data. PFNDAT provides the necessary information to characterize a wide variety of battle-induced and natural aerosols. Included in this collection are datasets describing four main classes of hazes (rural, maritime, urban, and tropospheric) at varying relative humidities; two types of fog (radiation and advection); rain at three precipitation rates (drizzle, moderate, and heavy); and two classes of snow ("dry" and "wet"). Dusts are treated under four categories: light, heavy, wind-lofted desert, and battlefield-induced high explosive munition. Inventory smokes include hygroscopic white phosphorus at three relative humidities, hexachloroethane, and fog oil. Finally, in the natural aerosol arena, the Navy Aerosol Model is provided for up-to-date modeling of the marine environment.

Providing scattering information in a database format allows aerosol scattering species to be used within larger radiative transfer models. The resulting propagation characteristics can readily be used within radiative transfer codes under a variety of conditions.

PFNDAT provides an accurate description of aerosol scattering properties for a wide range of particulates encountered on the dirty battlefield. This upgraded version, PFNDAT2006, provides significantly more resolution, detail, and versatility of aerosol species of interest to Army systems developers and radiative transfer specialists than previous editions have.

INTENTIONALLY LEFT BLANK.

1. Overview

Determining the amount of radiation transmitted through the atmosphere requires information on how the atmospheric constituents interact with that radiation. The aerosol Phase Function Database (PFNDAT) has been constructed to provide a significant part of this information. PFNDAT characterizes a wide variety of battle-induced and natural aerosols, including four classes of hazes (rural, maritime, urban, and tropospheric) at varying relative humidity levels; two types of fog (radiation and advection), each of which has a moderate and heavy aerosol loading; rain at three precipitation rates (drizzle, moderate, and heavy); two classes of snow ("dry" and "wet"); and four dust categories (light and heavy aerosol loading, wind-lofted desert, and dust raised by high energy munitions). It also uses the Navy Aerosol Model (NAM) for two air mass parameters, two average wind speeds, one current wind speed, and four relative humidities. Inventory smokes include white phosphorus (WP) at three relative humidities, hexachloroethane (HC), and fog oil.

This version, PFNDAT2006, corrects minor errors in the previous versions and extends the angular and wavelength resolution of most aerosols. The PFNDAT2006 results may also be used in other radiative transfer applications, such as solar loading and energy balance calculations.

If the user is interested in climate modeling, an excellent dataset consisting of aerosol properties averaged in space and time, along with a program to calculate the global distributions of optical or microphysical properties from the data files, may be found at http://www.lrz-muenchen.de/~uh234an/www/radaer/gads.html (*1*). A more detailed description is located in Koepke (*2*).

2. Introduction

2.1 The Phase Function and Associated Aerosol Parameters

The propagation of electromagnetic energy within the Earth's atmosphere depends on the wavelength of the radiation and on the nature of the medium being traversed. This medium consists of various molecular species and aerosol particles. These atmospheric particles, or aerosols, are ubiquitous in nature and frequently are the determining factor in the amount of radiation received at a sensor. At all wavelengths, aerosols generally scatter radiation out of the line-of-sight (LOS) into various angles. The probability of scattering per particle encounter is given by the single scattering albedo (ϖ_0). In contradistinction to ϖ_0, the angular probability distribution of scattering radiation, according to a direction relative to the incident radiation (i.e., the probability that an incident photon will be scattered into a particular angle θ relative to its initial direction of propagation), is given by the "phase function."

The phase function only provides information applicable to a single scattering event; in multiple scattering calculations, it is used repetitively. To calculate the phase function, the aerosol's composition, number density, size distribution, and refractive index at the wavelength under

consideration must be known; often the relative humidity (RH) must also be taken into account. Further, a given aerosol species frequently is composed of weighted sums of more than one particle type, as in the case of various dusts. In this document, we discuss the aerosol composition, number density, and size distribution components. Since refractive indices for the aerosol models may be found in the references contained in the aerosol model sections, they are not presented here. In view of the fact that many of the refractive indices and extinction coefficients, along with plots of the phase functions, were presented in previous versions of this database (*3*, *4*), we have included those documents on the distribution CD. The aerosol types, the range of meteorological parameters, and the wavelengths at which they were computed for PFNDAT2006 and previous versions are presented in table 1.

Table 1. Aerosol types contained in PFNDAT2006 and previous versions, along with their meteorological parameter range and wavelength resolution.

		Previous or PFNDAT2005			**PFNDAT2006**		
Aerosol Type ***Sub-type(s)***	**RH (%)**	**Number of Wavelengths**	**Wavelength (μm)**	**Delta (μm)**	**Number of Wavelengths**	**Wavelength (μm)**	**Delta (μm)**
Maritime	0 50 70 80 90 95 98 99	9	0.35–0.75	0.05	15	0.20–0.30	0.05
						0.3371	–
						0.35–0.60	0.05
						0.6328	–
						0.65–0.75	0.05
						0.86	–
		1	1.06	–	NC		
		5	3.0–5.0	0.50	NC		
		9	8.0–12.0	0.50	NC		
		8	14.0, 15.0, 18.0, 20.0, 25.0, 30.0, 35.0, 40.0	Variable	NC		
		Total = 32			Total = 38		
Urban	Same as above						
Rural	Same as above						
Tropospheric	Same as above						
Fog *Heavy and moderate: radiation and advection*	–	Same as above					
Rain *Drizzle, widespread, thunderstorm*	–	Same as above					
Snow *Wet and dry*	–	9	0.35–0.75	0.05	33	0.20–1.0	0.025
		1	1.06	–	NC NC NC NC		
		5	3.0–5.0	0.50			
		9	8.0–12.0	0.50			
		8	14.0, 15.0, 18.0, 20.0, 25.0, 30.0, 35.0, 40.0	variable			
		Total = 32			Total = 56		

NOTE: NC = no change

Table 1. Aerosol types contained in the PFNDAT2006 and previous versions, along with their meteorological parameter range and wavelength resolution (continued).

		Previous or PFNDAT2005			PFNDAT2006		
Aerosol Type *Sub-type(s)*	**RH (%)**	**Number of Wavelengths**	**Wavelength (μm)**	**Delta (μm)**	**Number of Wavelengths**	**Wavelength (μm)**	**Delta (μm)**
Desert-lofted dust *Wind speeds (m/s) 0 10 20 30*	–	Same as Maritime					
Dust *Light and heavy loading*	–	5	0.55–0.75	0.05	17	0.20–1.0[a]	0.05
		1	1.06	–	NC[a]		
		5	3.0–5.0	0.50	NC		
		9	8.0–12.0	0.50	NC		
		Total = 20			Total = 32		
High Explosive dust	–	Same as above			No change		
WP smoke	17 50 90	9	0.35–0.75	0.05	33	0.20–1.0	0.025
		1	1.06[b]	–	NC		
		5	3.0–5.0	0.50	NC		
		9	8.0–12.0	0.50	NC		
		1	14.0	–	NC		
		Total = 25			Total = 49		
Fog oil	50	Same as above					
HC smoke	85	Same as WP smoke			No change		
Navy aerosol *AMP = 3 & 8; $\overline{U}$ =3 & 8; U=12*	50 80 95 99	9	0.35–0.75	0.05	33	0.20–1.0	0.025
		1	1.06	–	NC		
		5	3.0–5.0	0.50	NC		
		9	8.0–12.0	0.50	NC		
		8	14.0, 15.0, 18.0, 20.0, 25.0, 30.0, 35.0, 40.0	Variable	NC		
		Total = 32			Total = 56		

NOTE: NC= no change, AMP is the air mass parameter, $\overline{U}$ is the average wind speed (m/s), and U is the current wind speed (m/s).

[a] Refractive indices updated.

[b] Imaginary index at 0% RH corrected (white phosphorus only).

Since computer run time and memory have been virtually eliminated as impediments to code execution, we present here a greatly expanded version of the phase function database.

Extinction coefficients, albedos, asymmetry factors, aerosol concentrations, and number densities are included in the phase function data files as functions of relative humidity and wavelength. Their values may be examined using the "aerosol_info" program located in the appendix and on the distribution CD. The user is cautioned that when interpolating the extinction within wavelength bands (0.20-0.75 μm, 3.0–5.0 μm, 8.0–40.0 μm) care must be taken: peaks or valleys in the extinction coefficient may easily be missed due to coarse wavelength resolution.

When performing these calculations, the following standard assumptions were made:

- The particles are assumed to be spaced far enough apart that radiation scattered by one particle does not affect how radiation is scattered from another particle. Therefore, each scattering event is independent.
- A Mie scattering code is assumed valid for predicting the behavior of each scattering species. The usage of a Mie scattering method assumes that the particles can be approximated as spherical in shape. This assumption is often made even for nonspherical particles, because in most cases the orientation of the particles is random since no external influences, such as strong magnetic fields or hydrodynamic forces, are present. Orientation averaging then produces nearly the same result as the assumption of sphericity.
- The scattering properties of a given type of particulate distribution can be represented by a weighted integral over the particle size distribution. This approach depends on the assumption of independent scattering, as discussed above.
- Polarization effects in both the incident radiation and the scattered fields have been ignored. Hence, the azimuthal and polar field components arising from the Mie scattering analysis have been merged into a single scattered flux statistic.
- The particulate size distribution is homogeneous over the volume concerned.

2.1.1 Extinctions and Albedos

Having determined the scattering properties of various aerosol species, one can then use these quantities to accurately calculate the scattering and absorption of radiation at a given wavelength as it passes through the atmosphere. As alluded to above, the relevant information needed to determine these radiation results includes the angular scattering probability distribution (P), the volume extinction coefficient (κ) (in length^{-1}), and the single scattering albedo (ϖ_0). The volume extinction coefficient κ, which determines the attenuation of the incident radiation, is composed of two parts:

- A scattering coefficient κ_s that describes the radiation scattered out of the LOS without a change in wavelength
- The absorption coefficient κ_a that describes the amount of radiation along the LOS that is converted into other forms of energy or that undergoes a change in wavelength

These two quantities are related to κ and ϖ_0 by

$$\varpi_0 = \kappa_s / (\kappa_s + \kappa_a); \kappa_s = \varpi_0 \kappa; \kappa_a = (1-\varpi_0) \kappa. \quad (1)$$

The albedo ϖ_0 represents the probability that interacting radiation will be scattered rather than absorbed: for pure scattering, $\varpi_0 = 1$, and for total absorption, $\varpi_0 = 0$. Making the assumption that the obscurant material properties are essentially uniform, we can relate the extinction coefficient to the transmission (T) by the Beer-Lambert law for monochromatic radiation,

$$T = e^{-\kappa L}, \tag{2}$$

where L is the path length under consideration.

Frequently in practical problems dealing with smokes, dust, and other aerosols that may vary dynamically over time and space, it is observed that the volume extinction coefficient tends to fall into ranges of about 0.001–100 km^{-1}. Under these conditions the "mass" extinction coefficient, denoted here as α, in units of $m^2\ g^{-1}$, is typically used, which is in contradistinction to the "volume" extinction coefficient κ, which has units of km^{-1}. Using the mass extinction coefficient, the transmission can be expressed as

$$T = e^{-\alpha\ CL}, \tag{3}$$

where the term concentration length (CL) is used for the total mass density integrated over the LOS. The concentration C is typically measured in $g\ m^{-3}$ and the path length L in units such that either α CL or κ L is dimensionless. In support of this application, the aerosol concentration of each species is computed and included in the database. The extinction coefficient can be related to the concentrations by combining equations 2 and 3.

Since smoke densities are frequently a function of time, a method for reassessing the extinction coefficient at different times is useful. This reassessment may be accomplished by comparing equations 2 and 3, and noting that

$$\alpha\ C = \kappa, \tag{4}$$

$$= N\ s, \tag{5}$$

where s is the extinction cross section per particle (unit area) and N is the particle number density in units of particles/unit volume. Equating equations 5 and 6, we find for the volume extinction coefficient:

$$\kappa = N\ s. \tag{6}$$

Thus, the volume extinction coefficient κ can be scaled as a function of time, if N (or the quantity α C) is known as a function of time.

2.1.2 Phase Function

Transmittance is important, because it quantifies when a received signal will be below some operational threshold of an electro-optical device, thereby directly affecting target acquisition. But transmittance is not the only quantity that determines the energy that is detected. Just as extinction removes energy along a path, multiple scattering can return some of that energy into

the LOS. Radiation from other external sources will also scatter into the LOS, affecting image contrast and/or impacting the system's dynamic range handling capabilities. The aerosol phase function is an essential ingredient in determining the amount of radiation scattered by the aerosol.

The angular scattering distribution (the phase function) gives the directional distribution of radiation scattered by the aerosol under consideration: the phase function is proportional to the probability that incoming radiation is scattered through a scattering angle θ into an element of solid angle dΩ. For incident unpolarized radiation, the phase function, as used here, is normalized as

$$\int_{4\pi} P(\theta)\, d\Omega = 1.0. \tag{7}$$

The angular resolution for the PFNDAT2006 phase functions are listed in table 2.

Table 2. Angular resolution (in degrees) of PFNDAT2006.

0.000	0.005	0.010	0.015	0.020	0.025	0.030	0.035	0.040	0.045	0.050
0.055	0.060	0.065	0.070	0.075	0.080	0.085	0.090	0.095	0.100	0.110
0.12	0.13	0.14	0.15	0.16	0.17	0.18	0.19	0.20	0.21	0.22
0.23	0.24	0.25	0.26	0.27	0.28	0.29	0.30	0.31	0.32	0.33
0.34	0.35	0.36	0.37	0.38	0.39	0.40	0.41	0.42	0.43	0.44
0.45	0.46	0.47	0.48	0.49	0.50	0.55	0.60	0.65	0.70	0.75
0.80	0.85	0.90	0.95	1.00	1.50	2.00	2.50	3.00	3.50	4.00
4.50	5.00	5.50	6.00	6.50	7.00	7.50	8.00	8.50	9.50	10.00
12.00	14.00	16.00	18.00	20.00	24.00	28.00	32.00	36.00	40.00	44.00
48.00	52.00	56.00	60.00	64.00	68.00	72.00	76.00	80.00	84.00	88.00
92.00	96.00	100.00	104.00	108.00	112.00	116.00	120.00	124.00	128.00	132.00
136.00	140.00	142.00	144.00	146.00	148.00	150.00	152.00	154.00	156.00	158.00
160.00	161.00	162.00	163.00	164.00	165.00	166.00	167.00	168.00	169.00	170.00
171.00	172.00	173.00	174.00	175.00	176.00	177.00	178.00	179.00	180.00	

2.1.3 Asymmetry Parameter

Simple approximations to the phase function are frequently sought for calculations where many scatterings have occurred and/or the optical depth is sufficiently large. One such approximation is the Henyey-Greenstein (HG) phase function (5):

$$P_{HG}(\theta, g) = \frac{1}{4\pi} \frac{1 - g^2}{(1 - 2g\cos(\theta) + g^2)^{3/2}}, \tag{8}$$

where g is called the asymmetry factor and is a relative measure of forward or backward scattering. This phase function is particularly appealing as it is dependent only on the single parameter g. For isotropic scattering, g is 0; for highly peaked phase functions, as is common at

visible wavelengths, *g* approaches its maximum value of 1. The asymmetry formulation also admits to a negative solution, where the phase function would be peaked in the reverse direction (180°). The asymmetry factor is defined as the average cosine of the scattering angle weighted by the phase function:

$$g = <\cos\theta> = \int_{4\pi} \cos\theta\, P(\theta)\, d\Omega \,/\, \int_{4\pi} P(\theta)\, d\Omega. \quad (9)$$

We have included values of g for all aerosols.

2.2 Particle Size Distribution Models

Aerosols are frequently a combination of more than one type; each type may have its own relative density distribution and refractive index properties. For example, typical dusts are assumed to be composed of various component quantities of quartz, montmorillonite, and ammonium sulfate particles. Each particle type has a particulate bulk density ρ in units of g cm^{-3} or as a dimensionless specific gravity. As mentioned above, each species may be characterized by a given mass concentration, C (g/cm^3), which represents the weight of lofted material mixed within a unit volume of air. From a meteorological standpoint, for aerosols comprised primarily of water, C is often referred to by the term "liquid water content." The term "mass concentration" is used to describe both effects in this text.

The quantities ρ and C are related by the particle size distribution, denoted by n(r), where r is the radius of a spherical particle. The total number of particles per unit volume is denoted by the number density N, which is related to the particle size distribution through

$$N = \int_0^\infty n(r)\, dr, \quad (10)$$

where n(r) has units of particles per cm^3-μm.

We may now write the mass concentration as a function of the particle size distribution,

$$C = 4/3\ \pi \int_0^\infty n(r)\, r^3\, \rho\, dr, \quad (11)$$

where $(4/3)\pi r^3\rho$ is the mass of a particle of radius r. The total mass concentration of a mixed aerosol is assumed to be a weighted sum of individual constituent parts.

The three aerosol particle size distributions (gamma, modified gamma, and lognormal) used in determining the phase functions are presented in more detail in sections 2.2.1–2.2.3.

2.2.1 Gamma Distribution

The gamma distribution, used by the rain and snow models, is given by the equation

$$n(r) = N_0\, r^m \exp(-\Lambda r), \quad (12)$$

where N_0 is the y intercept, Λ is the slope, m is the order of the gamma size distribution, and r is the radius.

Taking m = 0, we find the number density to be

$$N = N_0/\Lambda. \tag{13}$$

The mass concentration for this distribution can be expressed as

$$C = 4\pi\rho N_0\Gamma(4)/(3\Lambda^4) = 8\pi\rho N_0/\Lambda^4. \tag{14}$$

2.2.2 Modified Gamma Distribution

The modified gamma (MG) distribution, used by the fog models, is given by the equation

$$n(r) = r_c\, r^{\beta} \exp\,[-(\beta/\gamma)\ (r/r_c)^{\gamma}], \tag{15}$$

where r_c is the mode radius, and β and γ are fit coefficients of the distribution. By integrating equation 15, we find the number density

$$N = A\, B^{-(\beta-1)/\gamma}\, \Gamma[(\beta+1)/\gamma]\, \gamma^{-1}. \tag{16}$$

The mass concentration for this distribution can be expressed as

$$C = \frac{4}{3}\pi\rho\, r_c^3 N \frac{\Gamma[(\beta+4)/\gamma]}{\left(\frac{\beta}{\gamma}\right)^{3/\gamma}\Gamma[(\beta+1)/\gamma]}. \tag{17}$$

2.2.3 Lognormal Distribution

The lognormal distribution, used by the smoke, dust, rural, urban, maritime, tropospheric, desert, and the Navy aerosol models, is given by the equation

$$n(r) = \sum_{i=1}^{k} \left[\frac{N_i}{\sqrt{2\pi}\,\ln(10)\, r\,\sigma_i}\right] \exp\left[-\frac{(\log_{10} r - \log_{10} r_{gi})^2}{2\sigma_i^{\,2}}\right], \tag{18}$$

where r_{gi} is the distribution geometric mean radius (or mode radius) in μm, σ_i is the width of the distribution measured in $\log_{10}$ space (*3*, *5*), and N_i is the number density of the i^{th} component with r_{gi}. We note in passing that some Mie codes, in particular AGAUS, the code used for this work, use natural instead of common logs to specify this distribution. The mass concentration equation for this distribution is given by

$$C_i = 4/3\ \pi\rho N_i\, r_{gi}^{\,3} \exp\,[9/2(\ln(10)\sigma_i)^2]. \tag{19}$$

3. Aerosol Models

3.1 Maritime, Urban, Rural, and Tropospheric Models

The parameters for the maritime, urban, rural, and tropospheric aerosol models have been taken from Shettle and Fenn (*6*); they are bimodal lognormal (equation 18 with k = 2), with the mode radius varying as a function of relative humidity. The rural aerosol model consists of small and large rural distributions with correspondingly different indices of refraction. Similarly, the urban aerosol model consists of small and large urban distributions comprised of the rural aerosol in combination with carbonaceous aerosols, the latter having the same size distribution as both components of the rural aerosol. The maritime aerosol model consists of the small rural (continental) distribution along with a large particle oceanic distribution. The tropospheric model is identical to the rural model, but without the large particle component of that size distribution. The indices of refraction for the individual aerosols are listed in *Models for the Aerosols of the Lower Atmosphere and the Effects of Humidity Variations on Their Optical Properties* (*6*).

The number densities (rounded) for each mode of the maritime, urban, rural, and tropospheric distribution types along with the mode radii (r_g), variance (σ_g), and related liquid water content information are provided in tables 3–6 for the user who may wish to change the visibilities. The geometric mean variance, σ_g used herein, is related to σ by

$$\sigma = \log10(\sigma_g). \tag{20}$$

Table 3. Mode radii (r_g), standard deviation (σ_g), and number densities (N) as functions of relative humidity for the small and large modes of the maritime haze aerosol model.

	Relative Humidity (%)							
Parameter	**0**	**50**	**70**	**80**	**90**	**95**	**98**	**99**
r_g (S) (μm)	0.02700	0.02748	0.02846	0.03274	0.03884	0.04238	0.04751	0.05215
σ_g (S)	2.239	2.239	2.239	2.239	2.239	2.239	2.239	2.239
N (S) (cm^{-3})	38251	35129	27757	13902	9697	6976	4360	2948
r_g (L) (μm)	0.1600	0.1711	0.2041	0.3180	0.3803	0.4606	0.6024	0.7505
σ_g (L)	2.512	2.512	2.512	2.512	2.512	2.512	2.512	2.512
N (L) (cm^{-3})	386.4	354.8	280.4	140.4	98.0	70.5	44.0	29.8

NOTE: S = small and L = large.

Table 4. Mode radii (r_g), standard deviation (σ_g), and number densities (N) as functions of relative humidity for the small and large modes of the urban haze aerosol model.

	Relative Humidity (%)							
Parameter	**0**	**50**	**70**	**80**	**90**	**95**	**98**	**99**
r_g (S) (μm)	0.02500	0.02563	0.02911	0.03514	0.04187	0.04904	0.05996	0.06847
σ_g (S)	2.239	2.239	2.239	2.239	2.239	2.239	2.239	2.239
N (S) (cm^{-3})	87204	83354	64829	42776	27693	18217	10516	7286
r_g (L) (μm)	0.4000	0.4113	0.4777	0.5805	0.7061	0.8634	1.1691	1.4858
σ_g (L)	2.512	2.512	2.512	2.512	2.512	2.512	2.512	2.512
N (L) (cm^{-3})	10.9	10.4	8.1	5.4	3.5	2.3	1.3	0.9

NOTE: S = small and L = large.

Table 5. Mode radii (r_g), standard deviation (σ_g), and number densities (N) as functions of relative humidity for the small and large modes of the rural haze aerosol model.

	Relative Humidity (%)							
Parameter	**0**	**50**	**70**	**80**	**90**	**95**	**98**	**99**
r_g (S) (μm)	0.02700	0.02748	0.02846	0.03274	0.03884	0.04238	0.04751	0.05215
σ_g (S)	2.239	2.239	2.239	2.239	2.239	2.239	2.239	2.239
N (S) (cm^{-3})	79076	76305	70804	51674	33895	27052	19290	14761
r_g (L) (μm)	0.4300	0.4377	0.4571	0.5477	0.6462	0.7078	0.9728	1.1755
σ_g (L)	2.512	2.512	2.512	2.512	2.512	2.512	2.512	2.512
N (L) (cm^{-3})	9.9	9.5	8.9	6.4	4.2	3.4	2.4	1.9

NOTE: S = small and L = large.

Table 6. Mode radii (r_g), standard deviation (σ_g), and number densities (N) as functions of relative humidity for the tropospheric aerosol model.

	Relative Humidity (%)							
Parameter	**0**	**50**	**70**	**80**	**90**	**95**	**98**	**99**
r_g (μm)	0.02700	0.02748	0.02846	0.03274	0.03884	0.04238	0.04751	0.05215
σ_g	2.239	2.239	2.239	2.239	2.239	2.239	2.239	2.239
N (cm^{-3})	87180	84113	78115	56956	37152	29502	21673	16802

The hygroscopic aerosol mass concentration data is contained in table 7 and has been derived using equation 19. The extinction coefficients were generated for a meteorological visibility of 5.0 km; the number densities correspond to those found in tables 9–11 in reference 6.

Table 7. Hygroscopic aerosol mass concentration ($\mu g/m^3$) as a function of relative humidity for small mode, large mode, and total mass concentration for maritime, urban, rural, and tropospheric aerosols.

Aerosol Type	Relative Humidity (%)							
	0	**50**	**70**	**80**	**90**	**95**	**98**	**99**
Maritime								
Small	58.7	56.8	49.9	38.0	44.3	41.4	36.4	32.6
Large	301.7	338.7	454.4	860.5	1027.3	1313.0	1833.2	2400.9
Total	360.3	395.5	504.3	898.5	1071.6	1354.4	1869.7	2433.5
Urban								
Small	106.2	109.4	124.6	144.7	158.4	167.5	176.7	182.3
Large	133.0	137.9	168.3	201.3	234.8	282.1	395.8	561.7
Total	239.2	247.3	292.9	346.0	393.3	449.6	572.5	744.9
Rural								
Small	121.3	123.4	127.2	141.3	154.8	160.5	161.2	163.2
Large	150.0	151.8	162.0	200.4	216.0	229.8	421.1	588.9
Total	271.3	275.3	289.2	341.7	370.8	390.3	582.3	751.4
Tropospheric								
Total	133.7	136.0	140.3	155.8	169.7	175.0	181.2	185.7

3.2 Fog Models

Data from Shettle and Fenn (*6*) were also used for the fog models. In previous versions of PFNDAT, these models included only the heavy advection and moderate radiation. For this version, we have added two additional cases: moderate advection and heavy radiation. These models use the MG distribution (equation 15); the input parameters are listed in table 8 along with the mass concentrations (liquid water content) and number densities. According to Shettle and Fenn (*6*), these fogs are typical of radiation fogs and advection fogs, although they are also characteristic of developing and mature fogs, respectively.

Table 8. Mode radius (r_c),β, γ, A, B, N, and liquid water content for the fog aerosols.

Parameters	Fog Type			
	Heavy Advection	**Moderate Advection**	**Heavy Radiation**	**Moderate Radiation**
r_c (μm)	10	8	4	2
β	3	3	6	6
γ	1	1	1	1
A (particles/cm^3-cm)	.027	.06692	2.37305	607.5
B (cm^{-1})	.3	.375	1.5	3.0
N (particles/cm^{-3})	20	20	100	200
Liquid water content ($\mu g/m^3$)	372,300	190,636	62,553	15,640

3.3 The NAM

The NAM was developed in the 1980s (*7*) to describe the marine aerosol and its optical and infrared (IR) propagation properties for the atmosphere's marine boundary layer (MBL) using local meteorological parameters at shipboard level (nominally, 10 m). The model is a function of relative humidity, wind speed (24-h average and current), wavelength, and, implicitly, visibility. This model has no vertical structure, although such structure is being investigated (*8*, *9*). When the model is used in the MBL at levels away from the surface, it is assumed that the MBL is extremely well mixed and that the size distribution of the aerosol within this layer is constant from the sea surface to the top of the MBL.

The NAM is a four-component lognormal aerosol model, expressed as

$$\frac{dN}{dr} = \sum_{i=1}^{4} \frac{A_i}{f} \exp\left\{ - C\left[\ln(r/(f\ r_{0i})\right]^2 \right\}, \tag{21}$$

where dN/dr is the number of particles per cm^3 per micrometer; *i* is the component index; r is particle radius in micrometers; r_0 is the mode radius; $C = 1/(2\ \sigma^2)$, where $\sigma = 1/\sqrt{2}$ (therefore, C=1) is the standard deviation of the size distributions; A_i's are parameters fitted to the meteorological conditions and particle concentrations of the NAM component; and *f* is the effect of relative humidity given by the ratio of the particle radius at the ambient relative humidity to the particle radius at the standard relative humidity of 80% (*9*). The first and second components of equation 21 have the same mode radius, but are different classes of aerosols. The first class is a nonsoluble aerosol present only at high Air Mass Parameters (AMPs), and the second class is water soluble. Equation 21 can be related to equation 18 by noting that the geometric mean radius r_g used in equation 18 is equivalent to the median radius in NAM and is related to their mode radius by $r_g = r_{median} = r_{mode} \exp(\sigma^2)$, where the NAM form of the lognormal distribution has absorbed the r dependence into the exponential by modifying the A_i coefficients (*8*). Plots of the NAM number density as a function of radius may be found in *Optical Properties of the Marine Aerosol as Predicted by the Navy Aerosol Model* (*7*).

The original NAM used the hygroscopic growth formulization of Fitzgerald (*10*) for changes to the particle mode radii. Gerber (*11*) later extended Fitzgerald's relationship to particle sizes greater than 0.1 μm, relative humidities greater than 98%, and for varying properties of the different aerosol components. In Gerber's formulization, used in this work,

$$f = [(D - rh)/(E\ (1 - rh))]^{1/3}, \tag{22}$$

where rh is the relative humidity expressed in fractional form and f is the "growth factor" used for the hygroscopic growth of the particles in a humid environment. The NAM growth rule is designed around a baseline value such that f = 1.0 at 80% relative humidity for all aerosol types. The D's and E's in equation 22 take on the values in table 9 for the various NAM aerosol components.

Table 9. The D and E parameters and their humidity range for the NAM aerosol components.

NAM Component [a]	Aerosol Material	Mode Radii (μm)	D	E	Humidity Range (%)	Bulk Density (g cm^{-3})
1	Dust	0.03	NA	NA	NA	2.1
2	B1	0.03	1.17	1.87	< 99	1.86
3	Sea salt plus water	0.24	1.83	5.13	< 99.9	2.17
4	Sea salt plus water	2.0	1.97	5.83	< 99.99	2.17

[a]As used in this work.

The first component of the NAM is Shettle and Fenn's (*6*) dust-like aerosol, assumed to be nonsoluble; the second component is Volz's (*12*) B1 aerosol; and the third and fourth components are sea-salt water droplets and wave-generated sea water droplets. The mode radii for these components may be found in table 9. The first two components are considered to be background aerosols that are related to the AMP, which (as will be discussed below) is itself a function of relative humidity and transit time from point of origin. The third component is comprised of aerosols that have been produced by earlier high wind conditions that exhibit a relatively long residence time and, thus, are a function of the previous 24-h average of the wind speed. The fourth component, comprised of the largest aerosols, is considered to be related to the current wind speed and the current white water phenomenon. A more complete description of the components may be found in references 6 and 8. Finally, we modified our value of the bulk density for the first component (from 2.5 to 2.1 g cm^{-3}), resulting in different overall concentrations. The bulk densities used for components 2-4 may be found in table 9.

The number densities of the various aerosol components as a function of the AMP may be found using the following (*9*, *13*):

when AMP ≤ 5,

$$N_1 = 0 \text{ cm}^{-3}$$

$$N_2 = 136.55 \text{ AMP}^2 \text{ cm}^{-3}$$

when AMP > 5,

$$N_1 = 0.3 \times 136.55 \text{ AMP}^2 \text{ cm}^{-3}$$

$$N_2 = 0.7 \times 136.55 \text{ AMP}^2 \text{ cm}^{-3}$$

and for all AMP,

$$N_3 = 0.5462 \times \text{MAX}(5.866 \times (\overline{U} - 2.2), 0.5) \text{ cm}^{-3}$$

$$N_4 = 4.5518 \times 10^{(0.06\,U - 2.8)} \text{ cm}^{-3}$$

where $\overline{U}$ is the 24-h average wind speed (m/s) and U is the current wind speed (m/s).

The NAM refractive indices (*13*) are modified by Hänel's volume interpolation method (*14*):

$$m = m_w + (m_o - m_w)\,(f^3(0)/f^3(rh)), \tag{23}$$

where m_w is the refractive index of water and m_o is the refractive index of the dry aerosol.

We now have all the parameters necessary to determine the aerosol optical properties with the exception of the AMP, which describes the general condition of the air mass. An AMP of 1 indicates a pure air mass without contaminants and an AMP of 30 is the worse case situation that might be found downwind of a large industrial complex (*9*). There are four methods for determining the AMP parameter: 1) empirical judgment, 2) measurements related to MBL (i.e., the atmospheric radon content), 3) the elapsed time for the current air mass to reach the point of observation at sea from a distant land mass, or 4) analysis using the current wind speed, average wind speed, relative humidity, and visibility (*9*). Since none of these methods are easily obtainable for the typical user, we have instead initially taken values for the AMP and average wind speeds from the Target Acquisition Weapons Software (TAWS) (*15*). Available values in TAWS for AMP are 1, 5, or 10 and the available values for the average wind speeds are 3, 8, or 15 m/s. To complete the necessary input values, we have chosen current wind speeds of 0, 5, 12, and 20 m/s, and relative humidities of 50%, 80%, 95%, and 99%. Phase functions and extinction coefficients were calculated using these values at 32 wavelengths resulting in 4608 possible combinations. Since there are no existing published phase functions for NAM, we have compared the extinction coefficients generated using NAM6 (*13*) and AGAUS (*16*) for verification purposes. At 0.55 μm, the average error, using NAM6 as the "correct" value, was less than 1%: maximum errors, greater than 2% but less than 2.5%, were found at the 4 values of current wind speed (0, 5, 12, and 20 m/s) at a relative humidity of 50%, an AMP of 10, and an average wind speed of 15 m/s. Over all wavelengths, relative humidities, AMPs, $\overline{U}$'s, and U's, the average error was 2.8%.

3.3.1 Examination of the NAM Phase Functions

In the discussion that follows, we implicitly assume that the technique for calculating scattering effects will use a truncation method for the peak of the phase function, such as the delta-Eddington or small-angle approximation, that allows us to discount the forward peak values (0° to ~10°). In PFNDAT2005 (*17*) we examined the 144 phase function files to determine if there are similarities over the various AMPs, $\overline{U}$'s, and U's that would allow us to reduce this number. We made visual comparisons by plotting the phase functions at a wavelength of 0.55 μm with a relative humidity of 99%. An examination of these plots showed little variation in the phase function with current wind speed. Therefore, we opted to use only one current wind speed, arbitrarily chosen to be 12 m/s. To look for other possible reductions, a similar examination was performed holding the current wind speed constant at 12 m/s. Again visual inspection showed that there was little difference between 8 and 15 m/s for the average wind speed. Using the current wind speed of 12 m/s and average wind speeds of 3 and 8 m/s, this process was again repeated for AMPs of 1, 5, and 10. These results showed that there was little difference between AMPs of 5 and 10.

In this report, we further examine the above findings using the methodology of Kneizys et al. (*18*). We examined the rms difference (δ_{ij}) and the correlation (r_{ij}) parameters for all NAM phase function files in the set *ij* at a wavelength of 0.55 μm with a RH of 99%. Using correlation criteria of $r_{ij} \geq 0.98$ and $\delta_{ij} \leq 0.1$ and holding the AMP and $\overline{U}$ constant, U can meet these criteria by grouping results into a low U group (<12 m/s) and a high U group (≥12 m/s). Performing the same type of analysis keeping the AMP constant, but now breaking up the U into two groups ($U \geq 12$ m/s and $U < 12$ m/s), we find that the phase functions are well correlated for higher $\overline{U}$,

8–15 m/s; there is lesser agreement ($r_{ij} \approx 0.96$) at the lower $\overline{U}$. Finally, there is good correlation when the AMP only changes by one class (1–5 or 5–10). These results support the visual inspection findings and result in no change from PFNDAT2005.

Table 10 shows the values settled on for AMP, $\overline{U}$, and U at all wavelengths and relative humidities. This reduces the total number of phase functions from 4608 to 512 and the number of files from 144 to 16. Table 11 presents the meteorological visibilities associated with the selected NAM extinction coefficients; table 12 presents the concentrations and number densities for the selected AMP, $\overline{U}$, U, and relative humidities.

Table 10. Values selected for AMP, $\overline{U}$, and U for all wavelengths and relative humidities.

AMP		**Average Wind Speed, $\overline{U}$ (m/s)**		**Current Wind Speed, U (m/s)**	
Range	**Value**	**Range**	**Value**	**Range**	**Value**
$0 \le AMP < 4$	3	$0 \le \overline{U} < 8$	3	$0 \le U \le 20$	12
$4 \le AMP \le 10$	8	$8 \le \overline{U} \le 15$	8		

Table 11. Visibilities (km) for the selected NAM aerosols as a function of AMP; average and current wind speed (m/s); and RH.

Aerosol ID[a]	**AMP**	$\overline{U}$	**U**	**RH**			
				50%	**80%**	**90%**	**95%**
58–61	3	3	12	139	97	41	12
62–65	3	8	12	61	41	18	6.2
66–69	8	3	12	22	18	9.5	3.0
70–73	8	8	12	18	14	7.4	2.4

[a] For details of the aerosol ID ranges, see table 23.

Table 12. Concentrations and number densities for the selected NAM aerosols as a function of AMP; average and current wind speed; and RH.

Aerosol ID	**AMP**	$\overline{U}$ **(m/s)**	**U (m/s)**	**RH (%)**	**Concentration ($\mu g/m^3$)**	**Number Density (cm^{-3})**
58	3	3	12	50	2.498	1231.60
59	"	"	"	80	3.774	1231.60
60	"	"	"	90	10.15	1231.60
61	"	"	"	95	44.18	1231.60
62	3	8	12	50	3.988	1247.62
63	"	"	"	80	6.038	1247.62
64	"	"	"	90	16.28	1247.62
65	"	"	"	95	70.92	1247.62
66	8	3	12	50	4.758	8741.60
67	"	"	"	80	6.292	8741.60
68	"	"	"	90	13.97	8741.60
69	"	"	"	95	54.90	8741.60
70	8	8	12	50	6.248	8757.62
71	"	"	"	80	8.556	8757.62
72	"	"	"	90	20.10	8757.62
73	"	"	"	95	81.64	8757.62

3.4 Rain and Snow Models

The phase functions generated for rain and snow particle distributions are complicated by the large size parameters ($2\pi r/\lambda$) encountered. Because the size of these particles is very large, the amount of forward scatter due to diffraction can be extreme. According to Hodkinson and Greenleaves (*19*), when the airborne particles of an aerosol species are larger than a few wavelengths of the radiation being transmitted and a range of particle sizes or wavelengths exists, the combined single-scattering characteristics may be approximated by a combination of Fraunhofer diffraction, geometrical transmission, and reflection. While studying light scattering by irregular particles larger than the wavelength (such as snow), Hodkinson (*20*) found that, although the diffraction patterns of individual irregular particles vary greatly with shape, the resultant forward diffraction lobe for an ensemble of nonspherical particles with random orientations would be similar to an ensemble of spheres with cross-sectional areas equal to the particles' areas. Because the phase functions for typical rain and snow size distributions have sharp peaks in the forward direction, a set of angles concentrated in the forward direction were used for these phase functions. Otherwise, difficulties arise in the phase function interpolation processes. Both the rain and snow models use the gamma distribution (equation 12) with m = 0.

3.4.1 Rain Model

The most widely used analytical parameterization for raindrop size distribution is the gamma distribution, which has been found to realistically describe averaged raindrop size distributions in many parts of the world. Marshall and Palmer (*21*) proposed a simple negative exponential parameterization for the raindrop size distribution,

$$n(r) = N_0 \exp(-\Lambda r) = 1.6 \times 10^{-5} \exp(-8.2 \times 10^{-3} R^{-0.21} r) \ \text{cm}^{-3} \ \mu\text{m}^{-1}, \qquad (24)$$

as a fit to filter paper measurement of raindrop size spectra for rain rates (R) between 1 and 23 mm h^{-1}. Their parameterization has been found to remain a realistic representation of averaged raindrop size distributions for much higher rain rates. Uijlenhoet and Stricker (*22*), as the result of an analytical derivation based on a theoretical parameterization for the raindrop size distribution, found that

$$n(r) = N_0 \exp(-8.46 \times 10^{-3} R^{-0.214} r). \qquad (25)$$

They noted that the power law dependence between rainfall related variables is far from coincidental. Rather, it is a direct consequence of the fact that rainfall is not a continuous process, as is often assumed, but a discrete process consisting of individual raindrops with different sizes and fall speeds. The actual shape of the raindrop size distribution is determined by the relative magnitude of the competing microphysical processes, which lead to growth (coalescence, condensation) or decay (breakup, evaporation) of the raindrops as they fall to the ground (*23*). However, the measurement of small raindrops is close to the detection limit of many raindrop sampling devices and, moreover, small raindrops are more sensitive to the effects of wind, turbulence, and splash than large raindrops. Also for increasing rain rates, the proportion of large drops increases, and consequently, the proportion of small drops decreases.

Phase functions for rain were generated using a Marshall-Palmer particle size distribution with rain rates of 1, 5, and 10 mm/h, corresponding to rain types of drizzle, widespread, and thunderstorm, respectively. The number densities and liquid water content are given in table 13.

The Marshall-Palmer distribution yields somewhat larger particles at higher rain rates, causing the forward direction lobe of the phase function to be narrower and sharper. The phase functions given are considered to be reasonable for most rain conditions. Extinction for other rain rates may be calculated using the following (*24*),

$$\kappa = 0.51\ R^{0.63},\ km^{-1}\ \text{(drizzle)}, \tag{26}$$

$$\kappa = 0.36\ R^{0.63},\ km^{-1}\ \text{(widespread)}, \tag{27}$$

$$\kappa = 0.16R^{0.63},\ km^{-1}\ \text{(thunderstorms)}, \tag{28}$$

where R is in mm h^{-1}.

Table 13. Precipitation rates, number densities, and equivalent liquid water for the rain model.

Parameters	Precipitation Type		
	Rain Drizzle	**Rain Widespread**	**Rain Thunderstorm**
Rain rate (mm/hr)	1.0	5.0	10.0
Number density (particles/cm^3)	.001951	.00274	.00316
Liquid water content ($\mu g/m^3$)	89,000	344,000	616,000

3.4.2 Snow Model

The exact nature of snow size distributions is complicated by the size and shape of snow crystals, which are influenced by the temperature and humidity conditions that exist during their formation and growth. The basic crystal can also be modified by the attachment of super-cooled drops in a process called riming. These processes result in a wide variation in snow types with a subsequent large variation in associated visibilities. Because snow particle size distributions may vary greatly for a given snow rate, it is difficult to make generalizations about the scattering characteristics of a typical snow. Compounding this difficulty is the nature of the behavior of the refractive indices of ice, which are temperature, humidity, and wavelength dependent. Additionally no theory presently exists to calculate exactly the extinction coefficient for complex shapes such as snow crystals. Since the determination of snow phase functions is highly dependent upon the size distribution chosen and the determination of visibilities is not dependent upon the size distribution but is highly dependent upon the snow type, we have divided the following discussion into two sections: phase function determination and visibility determination.

Phase Function Determination

Calculations for the snow phase function and its associated scattering parameters use a gamma distribution (*25*) (cf., equation 12). The particle number density, precipitation rate, and equivalent liquid water content values, derived from equations presented in the "Visibility Determination" section, are given in tables 14 and 15. It should be noted that while the extinction coefficient is dependent on the number of particles, the phase function per se is not. For the snow size distribution used here, the size parameters in the visible range are large (>20,000) and Mie calculations are therefore suspect. In the mid- and far-IR the size parameter

is considerably smaller and Mie calculations, while still suspect, become more reasonable. Therefore, we have chosen to use Mie generated phase functions only in the mid- to far-IR. A hybrid approach comprised of fits to measured data combined with Mie calculations was used in the visible and near-IR.

Table 14. Independent parameters for the two snow types.

Snow Type	Λ (cm)	V_t (cm s^{-1})	C_3 (g cm^{-2})
Dry	20.1	100	0.017
Wet	17.7	200	0.072

Table 15. Dependent parameters for the two snow types (visibility = 3 km).

Snow Type	Do (cm)	κ (km^{-1})	ρ (g cm^{-3})	S (mm h^{-1})	N_0 (cm^{-3} cm^{-1})	N (cm^{-3})	Liquid Water Content ($\mu g/m^3$)
Dry	0.183	1.30	0.0929	0.265	0.0337	1.68×10^{-3}	60,300
Wet	0.207	1.30	0.348	2.25	0.0230	1.30×10^{-3}	256,000

To model the scattering properties at visible and near-IR wavelengths, we used Winchester's measured phase functions (*26*, *27*), covering a series of 5 snowfalls at a wavelength of 0.6238 μm (see figure 1). His measurements, which include propagation through large aggregates of snow particles, covered scattering angles from 10° to 170° and were normalized to a value of 1.0 at 10°. Scattering in this range, which is outside the forward peak region, essentially comprises geometric optic reflections and refractions within the particles. These geometric effects are relatively wavelength independent due to the large size parameters involved.

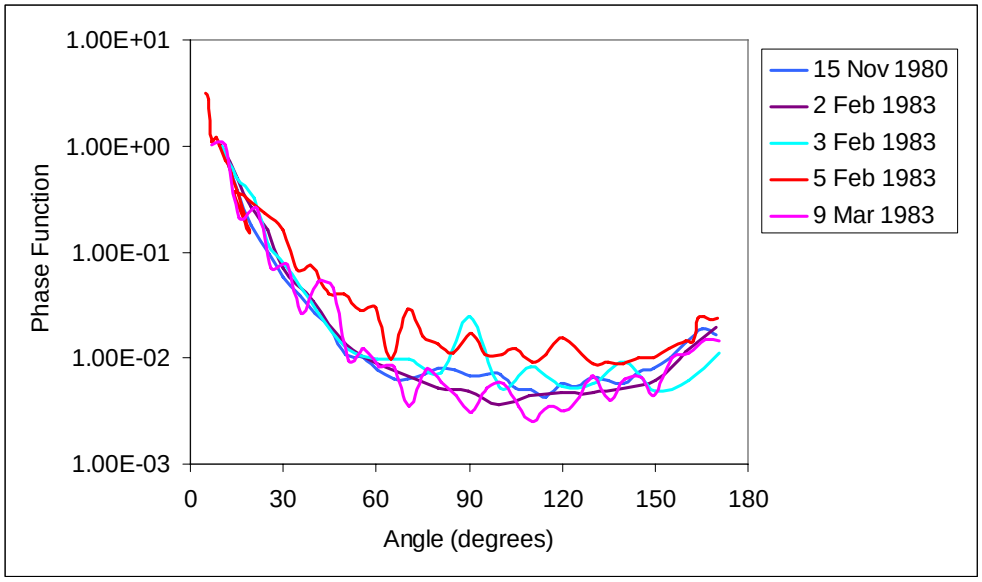

Figure 1. Snow phase function measurements taken by Winchester at 0.6238 μm.

To emulate these measurements, we fit the data to the 10° to 170° range and extended it to 180° using a set of three HG analytic phase functions. We then added a fourth HG phase function to reflect the forward peak.

The HG phase function is given by equation 8. The 4-term HG phase function can be written as

$$P_{HG}(\theta, g, a) = \sum_{i=1}^{4} a_i \frac{1 - g_i^{\,2}}{(1 - 2g_i \cos(\theta) + g_i^{\,2})^{3/2}}, \tag{29}$$

where the g_i are asymmetry parameters and the a_i are weighting coefficients: $\sum_{i=1}^{4} a_i = 1.0$.

The a_i's weight each HG term, which is appropriately peaked by the choice of g_i. We assume that the forward peak of the phase function, which is due to the diffraction pattern at these sizes, contains one-half of the energy (*28*). While not strictly true, we find that integration of our Mie generated phase functions from 0º to 1º contain approximately 50% of the area under the phase function curve. Since the first HG term will represent the forward peak, we assigned a weight of 0.5 to a_1. Knowing a_1, g_1 can be determined by setting the phase function at $\theta = 0°$ equal to the Mie computed peak value at 0° (A_{Mie}). Hence,

$$P_{HG}(0, g) = \frac{1}{4\pi} \frac{1 - g^2}{(1 - 2g + g^2)^{3/2}} = A_{Mie}. \tag{30}$$

Since g is required to be ≤ 1.0, we find the following equation for g_1:

$$g_1 = \frac{1 + 16\pi A_{Mie} - \sqrt{1 + 64\pi A_{Mie}}}{16\pi A_{Mie}}. \tag{31}$$

This formulation also allows the user to generate a phase function with a supplied peak value.

Additional guidance for the g_i's (i = 2-4) was found by noting that the second term should be peaked in the forward direction, the third term is isotropic, and the fourth term must be peaked in the backward direction. The a_i's were determined by fitting with the restriction that $\sum_{i=2}^{4} a_i = 0.5$.

Table 16 displays our final values. Thus the visible snow phase functions all have the same functional curve from 10° to 180°, but have different peak values at 0°, reflecting differences in the diffraction patterns. Finally, these hybrid phase functions were renormalized to one.

Table 16. Coefficients for the 4-term HG phase function.

i	**g_i**	**a_i**
1	~0.999 [a]	0.50
2	0.860	0.45
3	0.000	0.03
4	-0.600	0.02

[a]variable: determined by using equation 31.

Figure 2 presents the 4-term HG phase function, Winchester's data, and our Mie calculations interpolated to 0.6238 μm.

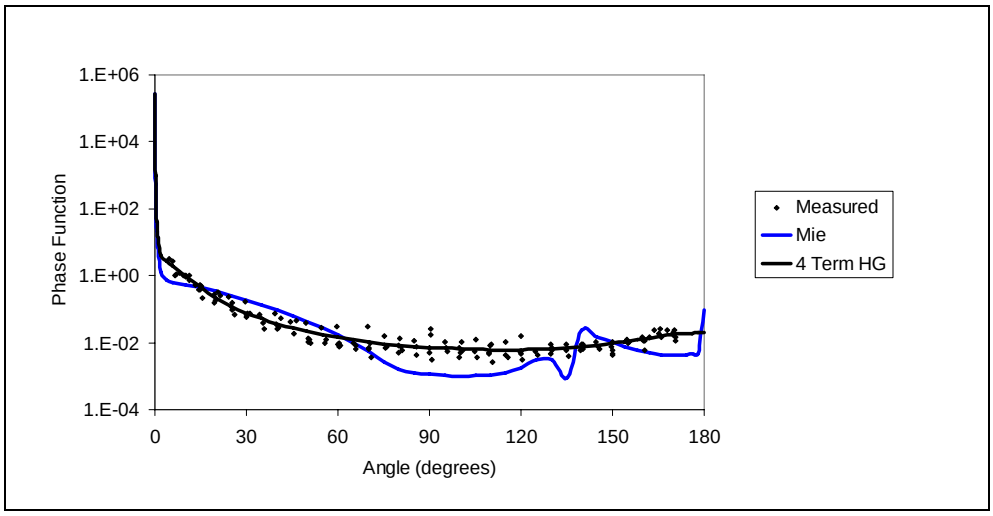

Figure 2. Phase function comparison of the 4-term HG (solid black) with the Mie (solid blue) at 0.6238 μm.

NOTE: Winchester's measurements are represented by the solid diamond shaped symbol (black).

We have compared the multiple scattering effects of the HG versus Mie phase functions by using the Monte Carlo code MSCAT (*29*). MSCAT predicts the direct, singly scattered, and multiply scattered laser radiation incident upon a detector viewing a homogeneous ellipsoidal aerosol cloud illuminated by a laser source. We chose a sensor with a 30° field of view looking directly along a "snow" cloud of optical depth 2.5, illuminated by a 0.6328-μm laser source elevated 45°, with azimuthal angles of 0°, 45°, 90°, 135°, and 180°. The sensor was placed at a 1-km distance from the cloud center to allow complete viewing of the cloud. The scenario is presented pictorially in figures 3 and 4; the results are presented in figure 5. In figure 5, we can see that there are significant differences in the radiation received, in agreement with the general shape of the phase functions per se. Even though the peaks of the Mie and HG phase functions are nominally the same, the "HG" received radiation is less, most likely due to the depressed scattering relative to the Mie function, between 20° and 60°. The radiance from 60° to 180° is in general agreement with the HG phase function being somewhat higher than the Mie function over this region.

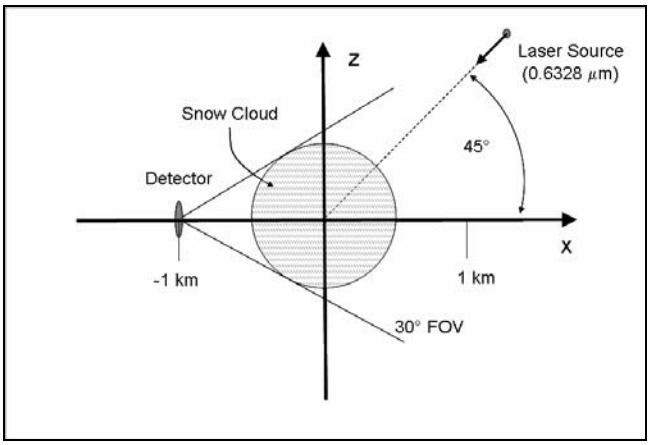

Figure 3. Horizontal view of scenario.

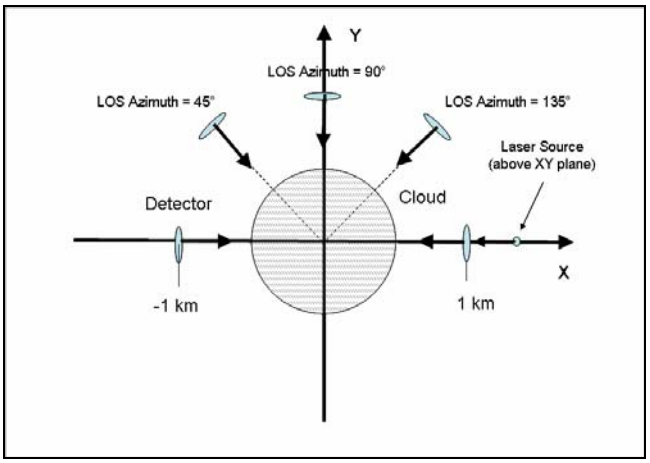

Figure 4. Downward view of scenario.

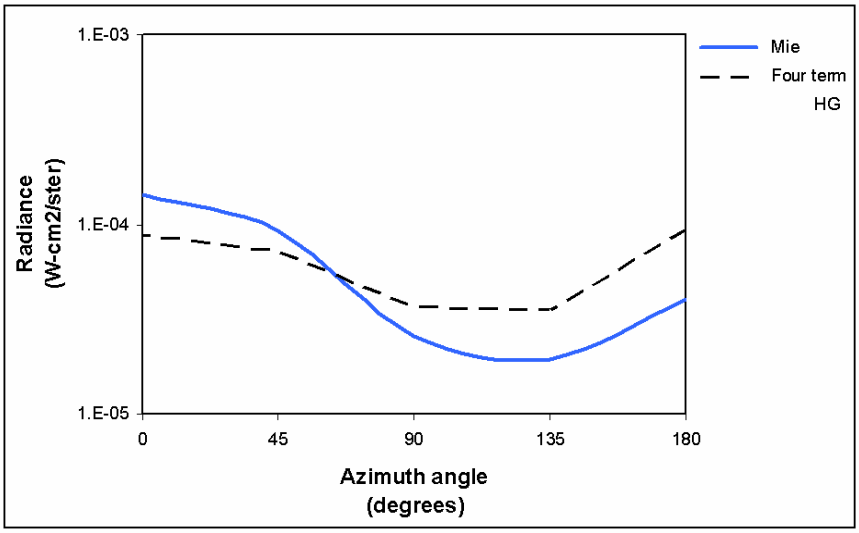

Figure 5. Received radiance from a 1-W laser source at 0.6328 μm passing through a simulated snow cloud.

NOTE: The solid line is the Mie generated phase function. The dashed line is the

4-term HG phase function.

Visibility Determination

1. Relation to liquid equivalent snow rate: Current methods of estimating operational snowfall intensity are based on prevailing visibility. The U.S. National Weather Service estimates of snow "intensity" are defined as follows: light snow intensity is reported when the visibility is greater than or equal to 1.0 km, moderate snow intensity is reported when the visibility is less than 1.0 km but greater than 0.5 km, and heavy snow intensity occurs when the visibility is less than or equal to 0.5 km. It has been shown (*30*) that this relationship frequently does not provide correct snowfall intensities, which is of particular concern to pilots. This visibility variation, leading to varying snowfall intensities, has been observed even though the liquid equivalent snowfall rate was constant. Liquid equivalent snowfall rate, hereafter referred to as "snowfall rate," is expressed as light when the snowfall rate is less than 1 mm h^{-1}, moderate when the snow rate is less than 2.5 mm h^{-1} but greater than 1 mm h^{-1}, and heavy when the snow rate is greater than 2.5 mm h^{-1}. Rasmussen et al. (*30*) have investigated the relationship between visibility and snow intensity and found that snow rate estimates may be greatly improved by considering time of day and snowfall type. We synopsize their findings below.

   There are many snow crystal types, their shape or habit being highly dependent upon the temperature and humidity in the cloud layer in which they are formed and whether or not these particles are being formed by deposition, aggregation, or riming. Riming is the freezing of super-cooled cloud droplets on snow crystals and is one of the fundamental snow growing mechanisms. Following the nomenclature of Rasmussen, we divide the snow into two general categories, wet and dry, which, excluding crystal types, covers almost all subsets of snow types. Generally, wet snow forms when the temperature is $\geq$-1 °C and can be further defined as partially melted and/or rimed. Assuming that snowflakes can be approximated by spheres, the density of these two snow types can be found by

$$\rho_{dry} = 0.17\ D^{-1}\ g\ cm^{-3}, \tag{32a}$$

   and

$$\rho_{wet} = 0.724\ D^{-1}\ g\ cm^{-3}, \tag{32b}$$

   where D is the snowflake diameter in mm. Daytime meteorological visibility is calculated from

$$V = 3.912/\kappa\ \ cm, \tag{33}$$

   where V is the visibility and κ is the volume extinction coefficient. Using the gamma distribution for the snow particle size, it can be shown that the extinction coefficient,

$$\kappa = \pi\ N_0/\Lambda^3\ cm^2\ cm^{-3}, \tag{34}$$

   where N_0 and Λ have been defined previously. Thus,

$$V = 1.245 \times 10^{-5} \Lambda^3/N_0 = 1.245 \times 10^{-5} \Lambda^2/N \text{ km}. \quad (35)$$

The visibility can also be related to the mass median diameter, D_0, by

$$V = 16.77/(D_0^2 N). \quad (36)$$

Therefore, knowing D_0, N can be determined from the visibility. Now, for the snow size distribution used here, it can be shown that the (liquid equivalent) snowfall rate is

$$S = \pi \rho N_0 V_t / \Lambda^4 \text{ cm s}^{-1}, \quad (37)$$

where V_t is the terminal snowflake velocity taken to be 100 cm s^{-1} for dry snow and 200 cm s^{-1} for wet snow. Since the density of water is 1 g cm^{-3}, the units of equation 38 can also be written as g cm^{-2} s^{-1}. Using equations 32, 36, and 37, we can now relate the snow rate to the visibility:

$$S_{dry} = 0.796 / V \text{ mm h}^{-1} \quad (38a)$$

or

$$S_{wet} = 6.74 / V \text{ mm h}^{-1}, \quad (38b)$$

where V is now in km. The wide range in visibility for a given snowfall rate is produced by two factors: 1) the smaller cross-sectional area of wet snowflake aggregates compared with that of dry snowflake aggregates of the same mass and 2) the higher terminal velocity of wet snowflake aggregates compared with that of the dry snowflake aggregates of the same mass (*30*). Thus, for a snow rate of 1 mm h^{-1}, the visibility can range from 0.8 to 6.7 km, over a factor of 8. Conversely, with a visibility of 3 km (the value used for our calculations), and subsequent "dry" and "wet" snow rates of 0.27 and 2.25 mm h^{-1}, the snow intensity varies from light to moderate. This clearly points out the trouble using just observed visibility to determine snow intensity and/or snow rate without considering additional parameters, e.g., N, D_0, ρ, or snow type.

We have determined a self-consistent set of parameters for the two snow types by taking the distribution slope, Λ, from Braham's (*24*) table 4 (1026 EST on 21 Jan and 0855 EST on 14 Jan, his figures 3 and 4), and the terminal velocity (V_t) and the constant (C_3) relating density to diameter from Rasmussen (*30*). These values are shown in table 15. Assuming a visibility of 3 km, we can then determine the dependent quantities, D_0, κ, ρ, S, N_0, and N from equations above. The dependent parameters, including the liquid water content, are presented in table 15.

2. Day/night effect: Rasmussen also investigated the effect of nightfall on the estimation of snowfall rate by visibility. The American Meteorological Society (*31*) defines visibility as "the greatest distance in a given direction at which it is just possible to see and identify with the unaided eye 1) in the daytime, a prominent dark object against the sky at the horizon, and 2) at night, a known, preferably unfocused, moderately intense light source." Daytime estimates of visibility are subjective evaluations of atmospheric attenuation of contrast, while nighttime estimates represent attempts to evaluate the attenuation of flux density. Rasmussen found that visibility-based estimates of snow intensity at night should

be increased by one category. Thus, during the night, light snow intensity should be increased to moderate, and moderate snow intensity should be increased to heavy as presented below in table 17 (Rasmussen's (*30*) table 6, reproduced with permission), and in a different format in table 18. To aid with visibility determination in wet or dry snow, these tables present snowfall intensity as a function not only of visibility, but also of temperature.

Table 17. Modified visibility criteria for snowfall intensity[a] (based on temperature and day or night).

<table>
<tr><th rowspan="2">Condition</th><th colspan="2">Temperature</th><th colspan="6">Horizontal Visibility (Statute Miles and [km])</th></tr>
<tr><th>°C</th><th>°F</th><th>¼ [0.4]</th><th>½ [0.8]</th><th>¾ [1.2]</th><th>1 [1.6]</th><th>1¼ [2.0]</th><th>> 1¼ [2.0]</th></tr>
<tr><td rowspan="2">Snow
Daylight
(Light > 3 ft candles)</td><td>< -1 °C</td><td>< 30 °F</td><td>Heavy</td><td>Moderate</td><td colspan="4">Light</td></tr>
<tr><td>≥ -1 °C</td><td>≥ 30 °F</td><td colspan="2">Heavy</td><td>Moderate</td><td colspan="3">Light</td></tr>
<tr><td rowspan="2">Snow
Nighttime
(Light < 0.5 ft candles)</td><td>< -1 °C</td><td>< 30 °F</td><td colspan="2">Heavy</td><td colspan="2">Moderate</td><td colspan="2">Light</td></tr>
<tr><td>≥ -1 °C</td><td>≥ 30 °F</td><td colspan="4">Heavy</td><td>Moderate</td><td>Light</td></tr>
</table>

NOTE: Rasmussen's (*30*) table 6, reproduced with permission.

[a] Light snowfall intensity is defined as less than 1 mm/hr equivalent liquid water precipitation, moderate snow as 1 mm/hr to 2.5 mm/hr, and heavy as greater than 2.5 mm/hr.

Table 18. Snow visibility (km) vs. snowfall intensity.

<table>
<tr><th rowspan="2">Condition</th><th colspan="2">Temperature</th><th colspan="3">Snowfall Intensity</th><th rowspan="2"></th></tr>
<tr><th>°C</th><th>°F</th><th>Heavy</th><th>Moderate</th><th>Light</th></tr>
<tr><td rowspan="2">Daylight</td><td>< -1</td><td>< 30</td><td>≤ 0.4</td><td>0.8</td><td>≥ 1.2</td><td rowspan="4">Visibility (km)</td></tr>
<tr><td>≥ -1</td><td>≥ 30</td><td>≤ 0.8</td><td>1.2</td><td>≥ 1.6</td></tr>
<tr><td rowspan="2">Nighttime</td><td>< -1</td><td>< 30</td><td>≤ 0.8</td><td>1.6</td><td>≥ 2.0</td></tr>
<tr><td>≥ -1</td><td>≥ 30</td><td>≤ 1.6</td><td>1.6 – 2.0</td><td>> 2.0</td></tr>
</table>

We have calculated scattering values for two types of snow, dry and wet, using the refractive indices for ice taken from Warren (*32*).

3.5 Dust Aerosol Models

3.5.1 Dust Model

Soil-derived aerosols are an important component of the total atmospheric aerosol content in certain geographic locations. Reported results of size distribution measurements for these aerosols vary widely. However, the general consensus is that the dust aerosols follow a bimodal lognormal distribution. Empirical data (*33*) fits this type of distribution well, and dust aerosols may be produced by a pulverization process in the soil. Epstein (*34*) has shown that such processes result in lognormal distributions. The bimodal distribution also provides a better fit, as empirical dust distributions appear to be characterized by more than one mode. Generally, the accumulation or small mode appears to be a characteristic of dust aerosols under all conditions, while the coarse or large mode is more a function of the parent soil size distribution (*33*). The latter component usually appears only under conditions of moderate to heavy aerosol dust loading.

The parameters for light and heavy aerosol loading (table 19) were taken at various locations, predominantly in the southwestern United States. Analyses of the small particle mode (*35*) showed that the constituents were primarily ammonium sulfate, carbon, calcite, sodium nitrate, quartz, and montmorillonite for both distributions. The particles contained in the large mode were seen to settle quickly, in both light and moderate cases, as the wind speed diminished. To allow the distribution to be more representative of varying geographic locations (*36*), the accumulation mode was considered to be comprised of 80% ammonium sulfate and 20% carbon by mass for the light aerosol loading case and 80% quartz and 20% montmorillonite by mass for the heavy aerosol loading.

Table 19. Values of lognormal particle size distributions parameters for the dust and high explosive (HE) dust models: bulk density, number density, mass loading, mode radius, and geometric standard deviation.

Dust Type	**Light Loading**		**Heavy Loading**		**HE Dust**	
Mode	**Small**	**Large**	**Small**	**Large**	**Small**	**Large**
Composition	Ammonium sulfate	Quartz	Montmorillonite	Quartz		
Bulk density (g/cm3)	1.769	2.32	2.5	2.32	2.5	2.5
Number density (cm^{-3})	1988	3.79	39.62	0.1128	200	0.07
Mass loading ($\mu g/m^3$)	16	40	1000	10000	15930	48680
r_g (μm)	0.05	0.5	0.5	15	0.5	22.5
σ_g	2.0	2.0	2.25	1.6	2.6	1.87
Composition	Carbon		Quartz			
Bulk density (g/cm3)	1.8		2.32			
Number density (cm^{-3})	488.5		1218.6			
Mass loading ($\mu g/m^3$)	4		4000			
r_g (μm)	0.05		0.5			
σ_g	2.0		1.6			

The refractive indices for quartz are from Hoock and Sutherland (*37*) and the refractive indices for ammonium sulfate are from Longtin et al. (*38*). Since the refractive indices of carbon have a large reported variablility (*39, 40*), we have used the indices for soot obtained from the software package Optical Properties of Aerosols and Clouds (OPAC) (*41, 1*). The refractive indices of montmorillonite from 0.20 to 1.06 μm are from the work of Arakawa et al. (*42*) and from 3.0 to 12.0 μm are from Hoock and Sutherland (*37*). The heavy loading dust type reflects very large mode radius constituents associated with high wind speeds. The light loading would be the case normally considered. Mixing the heavy and light cases should simulate intermediate condition dust cases. Because quartz is an optically positive uniaxial crystal (*43*), the scattering problem is divided into two parts. Two-thirds of the scattering material is treated using the ordinary indices of refraction. The remaining third of the material is treated using the extraordinary indices. It has been pointed out to the authors that the scattering properties at 0.55 μm for this phase function appear to be anomalous at higher wind speeds for backscatter angles greater than ~164° (cf., figure A-8b in reference 2). This appears to be a function of the quartz component of the aerosol (*44*, *45*) being increasingly lofted as the wind speed increases.

3.5.2 HE Dust Model

The HE dust model was generated using the empirical results of field tests (*46*) taken at Huntsville, AL, and Orogrande, NM. The results were empirically fitted to a bimodal lognormal curve with the parameters presented in table 19. The refractive indices were taken from the work of Ivlev and Popova (*47*). The refractive indices are synthetic spectra chosen because no consistent set of measurements covers the wavelength range in PFNDAT. A comparison of the synthesized spectrum with the measurements at the wavelengths available shows good agreement (*35*).

3.5.3 Vehicular Dust

The heavy, light, and HE dust models can, in some circumstances, be used for vehicular dust. The following is provided as guidance. The heavy and HE dust modes can be used for dust being raised by the vehicle; however, the coarse mode of these distributions will settle out in about 20 s, in which case the light dust model would be appropriate. The user is cautioned that soil types vary considerably and these models may not be representative of local soils. Refer to *The Infrared & Electro-Optical Systems Handbook* (*37*) for further information.

3.5.4 Desert Model

The characteristics of the desert aerosol model are detailed in Longtin et al. (*38*). This model arises from measurements taken in North Africa and the southwest United States between 1977 and 1985. The measurements included size distributions, composition, and total mass loading. The desert aerosol is comprised of three components; each component has a different lognormal particle size distribution and indices of refraction. The components represent carbonaceous particles, water soluble particles, and sand. Two types of sand contribute to the sand component: 50% of the sand particles are pure quartz and 50% are quartz contaminated with 10% hematite. The amount of carbonaceous and water soluble particles are constant (once scaled by the visibility), the sand component increases with wind speed. This model does not have humidity dependence.

While Longtin's data formed the baseline of these calculations, the Longtin data shows identical values for indices of refraction of pure quartz for the ordinary and extraordinary rays in both the visible and near-IR bands. More up-to-date information on quartz refractive indices was available in Hoock and Sutherland (*37*). The Hoock and Sutherland data showed distinctions in these values throughout the visible to far-IR bands and were used here as they were based on later, more accurate measurements. However, the Hoock and Sutherland data only go up to 12.0 μm; for wavelengths greater than 12.0 μm, we used Longtin's values. For the carbonaceous aerosol, we used the Longtin refractive indices, but we note that data from vegetative fires in Hoock and Sutherland show significant differences; however, these data are associated with aerosols extracted close to the source of emission and thus are battlefield aerosols in origin. Therefore the carbonaceous aerosols included here represent long-range atmospheric constituents with sources outside the immediate area.

For the water soluble (ammonium sulfate) refractive indices, we used Longtin's (*38*) values. The input parameters for the six distributions are presented in table 20. We used equation 19 to recover the number density based on known concentration values C. The number densities are in good agreement with those found by using Longtin's methodology. However, our number density for sand at 30 m/s wind speed differs from Longtin's due to an incorrect analytic volume: the correct volume is 5.978×10^{-5} μm^3. The data for the carbonaceous and water soluble aerosols (i.e., ammonium sulfate) are the same for each wind speed case, while the sand statistics vary. In our case, six aerosol components were necessary to accommodate the carbonaceous, water soluble, and four sand constituents: two each types of sand—pure quartz and 10% hematite contaminated quartz and two types of ray—ordinary (2/3rds) and extraordinary (1/3rd) with relative weightings as indicated. As a combined effect, we thus divided the total sand loading into 2/6ths ordinary ray pure quartz, 1/6th extraordinary ray pure quartz, 2/6ths ordinary ray 10% hematite contaminated quartz, and 1/6th extraordinary ray hematite contaminated quartz. Results obtained for extinction coefficients differ somewhat from those obtained by Longtin et al., primarily at shorter wavelengths due to the differing refractive indices.

Table 20. Particle size distribution parameters for desert aerosol components as a function of wind speed: bulk density, geometric mean radius, geometric standard deviation, number density, and mass loading.

Aerosol Component Type	**Carbonaceous**	**Water Soluble**	**Sand**			
Wind speed (m/s)	NA	NA	0	10	20	30
Bulk density (g/cm^3), ρ	2.00	1.77	2.65	2.65	2.65	2.65
Geometric mean (μm), r_g	0.0118	0.0285	6.24	7.76	9.28	10.80
Width parameter, σ_g	2.00	2.24	1.89	2.14	2.42	2.74
Number density (cm^{-3}), N	368.1	3,668.4	0.002442	0.01480	0.07113	0.31449
Mass loading (μg/m^3), C	0.044	11.70	39.68	1,012.5	20,555	413,066

3.6 Fog Oil, White Phosphorus, and Hexachloroethane Smoke Aerosol Models

The phase functions for inventory smokes can be calculated almost exactly, because the particles are nearly spherical. Discrepancies between theory and measurement can be attributed to uncertainties in the particle size spectrum or complex refractive indices. Experiments (*48*) have shown that the particle size spectrum is closely approximated by a lognormal distribution. Reference to the mass loading or mass concentration (C) of the particulate material (equation 11) rather than the number density is conventional in smoke applications. The extinction calculations have thus been performed for a constant aerosol loading factor of $1 g/m^3$ to permit scaling of results to arbitrary concentrations during simulations. The magnitude of C has no effect on the phase function or the mass extinction coefficient α, and only linearly scales the volume extinction coefficient κ (cf., equation 4). Table 21 lists the parameters considered representative of inventory smokes and includes the mass median diameter (MMD), often used in the literature in place of r_g. MMD is related to r_g and σ_g through the relation

$$\ln(MMD) = \ln 2r_g + 3\ln^2 \sigma_g, \tag{39}$$

where r_g and σ_g are listed in table 21. This table also shows that the mass concentration C was arbitrarily set to 10^6 $\mu g/m^3$.

Table 21. Representative parameters of inventory smokes at various relative humidities.

Aerosol Species	**WP**			**Fog Oil**	**HC**
RH (%)	17	50	90	50	85
Geometric mean (μm), r_g	0.241	0.269	0.365	0.190	0.422
Width parameter, σ_g	1.450	1.450	1.450	1.800	1.450
Bulk density (g/cm^3), ρ	1.617	1.443	1.178	0.890	1.220
Mass loading ($\mu g/m^3$), C	10^6	10^6	10^6	10^6	10^6
MMD	0.729	0.814	1.104	0.575	1.338

Table 21 also lists the particle spectrum parameters appropriate for fog oil dissemination by current military generators designed to produce particles most efficient for obscuration at visible wavelengths (*49*). Other experimental generators may produce larger particles. WP and HC have parameters listed for specific values of relative humidity. Hygroscopic growth has been modeled for these conditions by semi-empirical relations (*50*, *51*). Other evidence (*52*) shows that at high humidities (greater than 75% RH) a bimodal particle size spectrum may be expected that would be most pronounced for WP smoke.

The final considerations are the real and imaginary refractive indices. Hoock and Sutherland's (*37*) real and imaginary refractive indices for WP and fog oil were used. Reliable experimental measurements would be preferred, but such measurements are usually impossible because of the

complex reaction products formed in producing smoke (*53*). The values for selected wavelengths from the visible through the IR for HC were taken from Weast and Astle (*53*). They derived coefficients based on laboratory measurements performed on the major constituent of HC, zinc chloride (ZnCl2).

Fog oil smoke is not considered hygroscopic, so only a single dataset is used. In the visible, the imaginary index for fog oil is so small as to be beyond instrumental sensitivity; it can be considered negligible for most applications. This small value for the imaginary index leads to a single-scattering albedo of nearly unity, implying that extinction is entirely due to scattering.

Table 22 compares the average mass extinction coefficients (α) computed using the AGAUS Mie code (*16*), versus laboratory experimental results (*50–53*) for several spectral bands of interest. Since the measured results represent band averages, a typical cloud thickness of 0.01 km was assumed and results were computed by averaging the computed transmission through 1 g/m^3 density aerosols. Table 22 shows that all the comparisons are reasonable. Disparities are no larger than those found among various experiments throughout the above cited literature. Comparison of results for WP in the 8–12 μm region is sometimes taken as evidence that secondary reaction products are significant for WP smokes (*54*). The disparate results for fog oil at visible wavelengths may be due to the use of a single wavelength for the modeled results. Differences in the longwave IR band results may reflect different assumptions regarding sources. It is probably significant that the experimental data were obtained by the vapor condensation method rather than by pyrotechnic dissemination.

Table 22. Comparison of theoretical and experimentally measured mass extinction coefficients at 50% RH for various smoke aerosols.

λ (μm)	WP		Fog Oil		HC	
	Model	**Experiment**	**Model**	**Experiment**	**Model**	**Experiment**
visible[a]	4.282	3.940	5.367	7.730	3.227	4.579
1.06	1.963	1.410	3.737	3.500	2.601	2.040
3–5	0.284	0.290	0.262	0.270	0.193	0.190
8–12	0.284	0.366	0.021	0.014	0.068	0.052

NOTE: All mass extinction coefficients are given in m^2/g.

[a] 0.55 μm for the model; 0.4–0.7 μm for the experiment.

4. PFNDAT2006

There are 14 different aerosol classes contained in the database. These aerosols are functions of other parameters. The subtypes within a given aerosol class (advective, radiation fog, etc.) and RH, etc., result in 69 different aerosol variations. Each aerosol has a numerical ID associated with it (see table 23).

The database is comprised of a series of ASCII files, one for each of the aerosol identifiers (the numerical ID) listed in table 23. With the exception of the snow aerosol at visible and near-IR wavelengths, these phase functions and associated information were generated with AGAUS (*14*). Information relevant to the entire dataset has been placed on the first line, i.e., the phase function ID, the number of angles, the number of wavelength datasets, the aerosol concentration ($g\ m^{-3}$), the total number density ($particles/cm^3$), and the RH (%), formatted as (3(I3,1X), 2(E12.6,1X),F6.2). Where values were either not applicable or unknown, a value of -99.99 has been used as a placeholder. Following this are 153 discrete angles between 0º and 180º (cf., table 2), formatted as (22(F6.3,1X),131(F6.2,1x)). For backward compatibility, the last angle is followed by a sentinel number of 999.99. Following the angles is a one-line preamble comprised of the wavelength (μm), the single scattering albedo, the total volume extinction coefficient (km^{-1}), and the asymmetry parameter, formatted as (4(E12.6,1X)). Most of the aerosol types in PFNDAT2006 have had additional wavelengths added in the visible wavelength band. The reader is referred to table 1 for the complete set of wavelengths. Subsequent to this is the phase function, one value for each angle, at the wavelength under consideration, formatted as (6(E12.6,1X)). The total number of preambles and phase function sets in a given file corresponds to the "number of wavelength sets" read on the first line. The remainder of each file thus contains sets of aerosol scattering information (single scattering albedo, extinction, asymmetry, and phase function) for available wavelengths. The structure of these files is presented schematically in table 24. There is a blank between all data items, thereby allowing unformatted reads if so desired.

A FORTRAN90 computer program for interrogating all versions of the database is provided in the appendix and on the distribution CD.

Table 23. Aerosol ID as a function of aerosol type and RH.

Aerosol ID	RH (%)
1) Maritime	0
2) "	50
3) "	70
4) "	80
5) "	90
6) "	95
7) "	98
8) "	99
9) Urban	0
10) "	50
11) "	70
12) "	80
13) "	90
14) "	95
15) "	98
16) "	99
17) Rural	0
18) "	50
19) "	70
20) "	80
21) "	90
22) "	95
23) "	98
24) "	99
25) Fog (heavy advection)	NA
26) Fog (moderate radiation)	NA
27) Rain (drizzle)	NA
28) Rain (widespread)	NA
29) Rain (thunderstorm)	NA
30) Snow (dry)	NA
31) Fog (moderate advection)	
32) Fog (heavy radiation)	
33) Desert aerosol (ws=0)	
34) Desert aerosol (ws=10)	
35) Desert aerosol (ws=20)	
36) Desert aerosol (ws=30)	
37) Tropospheric	0

Aerosol ID	RH (%)
38) Tropospheric	50
39) Tropospheric	70
40) Tropospheric	80
41) Tropospheric	90
42) Tropospheric	95
43) Tropospheric	98
44) Tropospheric	99
45) Snow (wet)	
46) Reserved for future use	
47) Reserved for future use	
48) Reserved for future use	
49) Reserved for future use	
50) Dust (light loading)	NA
51) Dust (heavy loading)	NA
52) HE dust	NA
53) WP smoke	17
54) "	50
55) "	90
56) Fog oil	50
57) HC smoke	85
58) NAM (AMP=3, $\overline{U}$ =3,U=12)	50
59) "	80
60) "	95
61) "	99
62) NAM (AMP=3, $\overline{U}$ =8,U=12)	50
63) "	80
64) "	95
65) "	99
66) NAM (AMP=8, $\overline{U}$ =3,U=12)	50
67) "	80
68) "	95
69) "	99
70) NAM (AMP=8, $\overline{U}$ =8,U=12)	50
71) "	80
72) "	95
73) "	99

Table 24. Structure of an aerosol phase function data file.

PFN ID	**# θ's**	**# λ's**	**C**	**N**	**RH**
θ_1	θ_2		…		θ_{11}
θ_{12}	.		…	θ_{num_ang}	999.99
$\boldsymbol{\lambda_1}$	$\boldsymbol{\varpi_{01}}$	$\boldsymbol{\kappa_1}$	$\mathbf{g_1}$		
$P(\theta_1,\lambda_1,ID_1)$	$P(\theta_2,\lambda_1,ID_1)$	…	$P(\theta_6,\lambda_1,ID_1)$		
$P(\theta_{12},\lambda_1,ID_1)$		…	$P(\theta_{num\_ang},\lambda_1,ID_1)$		
$\boldsymbol{\lambda_2}$	$\boldsymbol{\varpi_{02}}$	$\boldsymbol{\kappa_2}$	$\mathbf{g_2}$		
$P(\theta_1,\lambda_2,ID_1)$	$P(\theta_2,\lambda_2,ID_1)$	…	$P(\theta_6,\lambda_2,ID_1)$		
$P(\theta_{12},\lambda_2,ID_1)$		…	$P(\theta_{num\_ang},\lambda_2,ID_1)$		
$\boldsymbol{\lambda_{max}}$	$\boldsymbol{\varpi_{0max}}$	$\boldsymbol{\kappa_{max}}$	$\mathbf{g_{max}}$		
$P(\theta_1,\lambda_{max},ID_1)$	$P(\theta_2,\lambda_{max},ID_1)$	…	$P(\theta_6,\lambda_1,ID_1)$		
$P(\theta_{12},\lambda_{max},ID_1)$		…	$P(\theta_{num\_ang},\lambda_{max},ID_1)$		

NOTE: PFN ID = phase function identifier from table 23
# θ's = total number of angles (cf., num_ang below)
# λ's = total number of wavelengths for this ID
C = concentration (g m^{-3})
N = particle density (cm^{-3})
RH = relative humidity (%)
θ_i = discrete angles (degrees)
λ_j = discrete wavelengths (μm)
ϖ_{0j} = albedo for single scattering at wavelength j
κ_j = extinction coefficient (km^{-1}) at wavelength j
g_j = asymmetry parameter at wavelength j
$P(\theta_i,\lambda_j,ID_1)$ = the value of the phase function at angle i, wavelength j, and aerosol type identifier I
num_ang = number of angles: 2006 = 153; 2005 and previous = 65

References

1. The software package OPAC (Optical Properties of Aerosols and Clouds), Hess, M. http://www.lrz-muenchen.de/~uh234an/www/radaer/opac.html (accessed July, 2006).
2. Koepke, P.; Hess, M.; Schult, I.; Shettle, E.P. *Global Aerosol Data Set*; Report No. 243; Max-Planck-Institut für Meteorologie: Hamburg, Germany, ISSN 0937-1060, 1997.
3. Shirkey, R.C.; Sutherland, R.A.; Seagraves, M.A. *EOSAEL 87 Volume 26 Aerosol Phase Function Data Base PFNDAT*; ASL-TR-0221-26; U.S. Army Atmospheric Sciences Laboratory: White Sands Missile Range, NM, 1987.
4. Tofsted, D.H.; Davis, B.T.; Wetmore, A.E.; Fitzgerrel, J.; Shirkey, R.C.; Sutherland, R.A. *EOSAEL 92 Aerosol Phase Function Data Base PFNDAT*; ARL-TR-273-9; U.S. Army Research Laboratory: White Sands Missile Range, 1997.
5. Henyey, L.C.; Greenstein, J.L. Diffuse radiation in the galaxy. *Astrophys. J.* **1941,** *93*, 70–83.
6. Shettle E.P.; Fenn, R.W. *Models for the Aerosols of the Lower Atmosphere and the Effects of Humidity Variations on Their Optical Properties*; AFGL-TR-79-0214; Air Force Geophysics Laboratory: Hanscom Air Force Base, MA, 1979.
7. Gathman, S.G. Optical Properties of the Marine Aerosol as Predicted by the Navy Aerosol Model. *Opt. Eng.* **1983**, *22*, 57-62.
8. Gathman, S.G.; van Eijk, A.M.J.; Cohen, L.H. *Characterizing Large Aerosols in the Lowest Level of the Marine Atmosphere*, Proceedings of SPIE vol. 3433, Propagation and Imaging through the Atmosphere II; L.R. Bissonnette, Ed.; pp 41–52, 1998.
9. Gathman, S.G.; Davidson, K.L. *The Navy Oceanic Vertical Aerosol Model*; NRaD Technical Report 1634; Naval Research And Development: San Diego, CA, December 1993.
10. Fitzgerald, J.W. *On the Growth of Aerosol Particles with Relative Humidity*; NRL Memorandum Report 3847; Navy Research Laboratory: Washington, D.C., 1978.
11. Gerber, H.E. *Relative Humidity Parameterization of the Navy Aerosol Model (NAM)*; NRL Report 8956; Navy Research Laboratory: Washington, D.C., December 1985.
12. Volz, F.E. Infrared Refractive Index of Atmospheric Aerosol Substrates. *Applied Optics* **1972,** *11*, 755–759.
13. Zeisse, C. *NAM6: Batch code for the Navy Aerosol Model*; SPAWAR Systems Center Technical Report 1804; October 1999 (http://sunspot.spawar.navy.mil/2858/software/).
14. Hänel, G. The Properties of Atmospheric Aerosol Particles as Functions of Relative Humidity at Thermodynamic Equilibrium with the Surrounding Moist Air. *Adv. Geophys.* **1976**, *19*, 73–188.

15. Shirkey, R.C.; Gouveia, M. Weather Impact Decision Aids: Software to Help Plan for Optimal Sensor and System Performance. *Crosstalk, J. of Defense Software Engineering*, **2002**, *15* (12), 17–21.

16. Miller, A. *Mie Code AGAUS 82*; ASL-CR-83-0100-3; U.S. Army Atmospheric Sciences Laboratory: White Sands Missile Range, NM, 1983.

17. Shirkey, R.C.; Tofsted, D.H. *Electro-Optical Aerosol Phase Function Database PFNDAT2005*; ARL-TR-3684; U.S. Army Research Laboratory: White Sands Missile Range, NM, 2005.

18. Kneizys, F.X; Shettle, E.P.; Gallery, W.O.; Chetwynd, Jr., J.H.; Abreu, L.W.; Selby, J.E.A.; Clough, S.A.; Fenn, R.W. *Atmospheric Transmittance/Radiance: Computer Code LOWTRAN6*; Technical Report 83-0187 (ADA137786); Air Force Geophysics Laboratory: Hanscom Air Force Base, MA, 1983.

19. Hodkinson, J.R.; Greenleaves, L. Computations of Light Scattering and Extinction by Spheres According to Diffraction and Geometrical Optics. *J. of the Optical Society of America* **1963,** *53*, 577–588.

20. Hodkinson, J.R. "Light Scattering and Extinction by Irregular Particles Larger than the Wavelength" in *Electromagnetic Scattering*, M. Kerker, ed.; Macmillan: New York, 1963.

21. Marshall, J.S.; Palmer, W.M. The Distribution of Raindrops with Size. *J. Meteorology* **1948**, *5*, 165–166.

22. Uijlenhoet, R.; Stricker, J.N.M. A consistent rainfall parameterization based on the exponential raindrop size distribution. *J. of Hydrology*, **1999**, *218*.

23. Pruppacher, H.R.; Klett, J. D. *Microphysics of Clouds and Precipitation*; D. Reidel Publishing: Boston, MA, 1980.

24. *Quantitative Description of Obscuration Factors for Electro-Optical and Millimeter Wave Systems*, Department of Defense Military Handbook, DOD-HDBK-178(ER), 1986.

25. Braham, R.R., Jr. Snow Particle Size Spectra in Lake Effect Snows. *J. of Applied Meteorology* **1990**, *29* (3).

26. Winchester, L.W., Jr.; Jackovich, J.E.; Hanson, N.K. *Phase Function Measurements at SNOW-TWO*, SNOW-TWO Data Report, v1; U.S. Army Corps of Engineers Cold Regions Research & Engineering Laboratory Special Report 84-20; R. Jordan, ed., Hanover, NH, June 1984.

27. Winchester, L.W., Jr.; Hanson, N.K.; Jackovich, J.E. *Phase Function Measurements of Snow Crystals*, Proceedings of the Snow Symposium III, v1, U.S. Army Corps of Engineers Cold Regions Research & Engineering Laboratory Special Report 83-31; Hanover, NH, 1983.

28. van de Hulst, H.C. *Light Scattering by Small Particles*, Dover Publications: New York, NY, 1981.

29. O'Brien, S.G. *Aerosol Multiple Scattering Module MSCAT*; ASL-TR-0221-19; Atmospheric Sciences Laboratory: White Sands Missile Range, NM, 1987.

30. Rasmussen, R.M.; Vivekanandan, J.; Cole, J. The Estimation of Snowfall Rate Using Visibility. *J. of Applied Meteorology* **1999**, *38* (10).

31. *Glossary of Meteorology*, T.S. Glickman, Ed.; American Meteorological Society: Boston, MA, 2000.

32. Warren, S.G. Optical constants of ice from the ultraviolet to the microwave. *Applied Optics* **1984**, *23* (8).

33. Patterson, E.M.; Gillette, D.A. Commonalities in Measured Size Distributions for Aerosols Having a Soil-Derived Component. *J. of Geophysics Research* **1977**, *82*, 2074–2082.

34. Epstein, B. The Mathematical Description of Certain Breakage Mechanisms Leading to the Logarithmic-Normal Distribution. *J. of the Franklin Institute* **1947**, *244*, 471–477.

35. Jennings, S.G.; Pinnick, R.G.; Auvermann, H. J. Effects of Particulate Complex Refractive Index and Particle Size Distribution Variations on Atmospheric Extinction and Absorption for Visible Through Middle IR Wavelengths. *Applied Optics* **1978**, *17*, 3922–3928.

36. Gillespie, J.B.; Lindberg, J.D. Seasonal and Geographic Variations in Imaginary Refractive Index of Atmospheric Particular Matter. *Applied Optics* **1992**, *31*, 2107–2112.

37. Hoock, D.W.; Sutherland, R.A., "Obscuration Countermeasures," chapter 6 of Countermeasure Systems, Volume 7, of *The Infrared & Electro-Optical Systems Handbook*; SPIE Optical Engineering Press: Bellingham, WA, 1996, pp 359–492.

38. Longtin, D.R.; Shettle, E.P.; Hummel, J.R.; Pryce, J.D. *A Wind Dependent Desert Aerosol Model: Radiative Properties*; AFGL-TR-88-0112; Air Force Geophysics Laboratory: Hanscom Air Force Base, MA, 1988.

39. Bond, T C.; Bertstrom, R.W. Toward Resolution on the Optics of Light-Absorbing Carbon. *Eos Trans. AGU* **2004**, *85* (47), Fall Meet. Suppl., Abstract A43E-07.

40. Toward Resolution on the Optics of Light-Absorbing Carbon, Bond, T C.; Bertstrom, R.W. http://cee.uiuc.edu/research/bondresearch/Bond_Resolution_AGU.pdf (accessed July 2006).

41. Hess, M.; Koepke, P.; Schult I. Optical Properties of Aerosols and clouds: The software package OPAC. *Bull. Am. Met. Soc.* **1998**, 79, 831–844.

42. Arakawa, E.T.; Tuminello, P.S.; Khare, B.N.; Milharn, M.E.; Authier, S.; Pierce, J. *Measurement of Optical Properties of Small Particles*, 1997 Scientific Conference on Obscuration and Aerosol Research, Aberdeen Proving Ground, MD, 1997, (http://www.osti.gov/bridge/product.biblio.jsp?osti_id=627449&query_id=0).

43. Born, M.; Wolf, E. *Principles of Optics*, 5th ed.; Pergamon Press: Oxford, UK, 1975.

44. Liu, L.; Mishchenko, M.I.; Hovenier, J.W.; Volten, H.; Muñoz, O. Scattering matrix of quartz aerosols: comparison and synthesis of laboratory and Lorenz–Mie results. *J. of Quantitative Spectroscopy & Radiative Transfer* **2003**, *79–80*, 911–920.

45. Haltrin, V.I.; Shybanov, E.B. *Light scattering properties of quartz particles in seawater*, Proceedings of the IEEE Geoscience and Remote Sensing Society 2000 Conference, Honolulu, HI, 2000, p1842–1844.

46. Pinnick, R.G.; Fernandez, G.; Hinds, B.D. Explosion Dust Particle Size Measurements. *Applied Optics* **1983**, *22*, 95–102.

47. Ivlev, L.S.; Popova, S.I. The Complex Refractive Indices of Substances in the Atmosphere-Aerosol Dispersed Phase. *Atmospheric and Oceanic Physics* **1973**, *9*, 587–591.

48. Jennings, S.G.; Gillespie, J.B. *Mie Theory Sensitivity Studies – The Effects of Aerosol Complex Refractive Index and Size Distribution Variations on Extinction and Absorption Coefficients*; ASL-TR-0003; U.S. Army Atmospheric Sciences Laboratory: White Sands Missile Range, NM, 1978.

49. Carlon, H.R. et al. Infrared Extinction Spectra of Some Cannon Liquid Aerosols. *Applied Optics* **1977**, *1b*, 1598–1605.

50. Frickel, R.H.; Rubel, G.O.; Stuebing, E.W. *Relative Humidity Dependence of the Infrared Extinction by Aerosol Clouds of Phosphoric Acid* (UNCLASSIFIED), Proceedings of Smoke Symposium III (U), CONFIDENTIAL, PM Smoke/Obscurants, Aberdeen Proving Ground, MD, 1979.

51. Rubel, G.O., *Predicting the Droplet Size and Yield Factors of a Phosphorus Smoke as a Function of Droplet Composition and Ambient Relative Humidity Under Tactical Conditions*; ARCSL-TR-78057; Chemical Systems Laboratory: Aberdeen Proving Ground, MD, 1978.

52. Farmer, W. M. *An Evaluation of Data Obtained During the H3S Test*, Proceedings of Smoke Symposium IV, Adelphi, MD, 1980, p 49–86.

53. Weast, R.C.; Astle, M.J., eds., *CRC Handbook of Chemistry and Physics*, 61st ed.; CRC Press: Boca Raton, FL, 1980-1981.

54. Milham, M.E. et al. *New Findings on the Nature of WP/RP Smokes*; ARCSL-TR-77067; Chemical Systems Laboratory: Aberdeen Proving Ground, MD, 1977.

INTENTIONALLY LEFT BLANK

Appendix: A FORTRAN90 Program for Interrogating the Phase Function Files

```
      program aerosol_info     ! Rev date: 7/14/06

c  Purpose:  This interactive program will read any PFNDAT phase function file
c    at the requested wavelength (interpolation is not performed) and print out
c    the parameters listed below.  PFNDAT 2005/2006 have different angular
c    resolutions (65 angles vs 153 angles, respectively).  PFNDAT2006 also has two
c    versions: "a" and "b".  Both have the same number of angles (153), but
c    different wavelength resolution - the "b" version has additional
c    wavelengths.  PFNDAT 87/92 output values do not include relative humidity*,
c    particle concentration or number density.  The integral of the phase function
c    is also computed by this program.  For additional information see the references below.

c  Phase function normalization can be determined by integrating it
c    over all angles:
c
c          2pi pi
c           / /
c           | | P(cos(theta)) sin(theta) d(theta) d(phi)
c           / /
c           0 0
c
c    the asymmetry factor has an additional factor of cos(theta)

c  Note: the integral of the phase function and the asymmetry are highly
c    dependent upon the angular resolution of the phase function.  This
c    is particularly so when the phase function is highly peaked.

c  Usage:
c    The program is interactive: relevant wavelength and file name are requested.
c    The user can optionally have the phase function and associated angles
c    printed out.  The program will attach the requested phase function file to
c    unit "udat".  Maximum input file name length is 9 characters.

c  Input:
c    Wavelength (um) [input value of 0 will examine all wavelengths in the file]
c    Name of phase function data file to be examined

c  Output:
c    angles (degrees)  [optional]
c    phase function(s) at requested wavelength(s) [optional]
```

```
c    wavelength (microns)
c    single scattering albedo
c    extinction coefficient (km-1)
c    scattering coefficient (km-1)
c    absorption coefficient (km-1)
c    asymmetry parameter (see note above)
c    integral of phase function  (see note above)
c    relative humidity(%) [*2005/6 only; for PFNDAT87/92 see tables in references]
c    particle concentration (g/m**3)  [2005/6 only]
c    number density (particles/cc)    [2005/6 only]

C  AEROSOL TABLE
c
C  ID  Aerosol Type                    rh
C
C  0) USER SUPPLIED
C  1) MARITIME                        0%
C  2)       "                         50%
C  3)   "                             70%
C  4)   "                             80%
C  5)   "                             90%
C  6)   "                              95%
C  7)   "                             98%
C  8)   "                             99%
C  9) URBAN                           0%
C  10)   "                            50%
C  11)   "                            70%
C  12)   "                            80%
C  13)   "                            90%
C  14)   "                            95%
C  15)   "                            98%
C  16)   "                            99%
C  17) RURAL                          0%
C  18)   "                            50%
C  19)   "                            70%
C  20)   "                            80%
C  21)   "                            90%
C  22)   "                            95%
C  23)   "                            98%
C  24)   "                            99%
C  25) FOG (HEAVY ADVECTION)          NA
C  26) FOG (MODERATE RADIATION)       NA
C  27) RAIN (DRIZZLE)                 NA
C  28) RAIN (WIDESPREAD)              NA
C  29) RAIN (THUNDERSTORM)             NA
C  30) SNOW (dry)                     NA
```

```
c  31) Fog (moderate advection)          NA
c  32) Fog (heavy radiation)             NA
c  33) Desert aerosol (ws=0)             NA
c  34) Desert aerosol (ws=10)            NA
c  35) Desert aerosol (ws=20)            NA
c  36) Desert aerosol (ws=30)            NA
c  37) Tropospheric                      0%
c  38) Tropospheric                      50%
c  39) Tropospheric                      70%
c  40) Tropospheric                      80%
c  41) Tropospheric                      90%
c  42) Tropospheric                      95%
c  43) Tropospheric                      98%
c  44) Tropospheric                      99%
C  45) SNOW (wet)                       NA
C  46) - 49) (RESERVED FOR FUTURE USE)
C  50) DUST (LIGHT LOADING)             NA
C  51) DUST (HEAVY LOADING)             NA
C  52) HIGH EXPLOSIVE (HE) DUST         NA
C  53) WP SMOKE                         17%
C  54)   "                              50%
C  55)   "                              90%
C  56) FOG OIL                          50%
C  57) HC SMOKE                         85%
c  58) NAM   (AMP=3,ubar=3,U=12)        50%
c  59)          "                      80%
c  60)          "                      95%
c  61)          "                      99%
c  62) NAM   (AMP=3,ubar=8,U=12)        50%
c  63)          "                      80%
c  64)          "                      95%
c  65)          "                      99%
c  66) NAM   (AMP=8,ubar=3,U=12)        50%
c  67)          "                      80%
c  68)          "                      95%
c  69)          "                      99%
c  70) NAM   (AMP=8,ubar=3,U=12)        50%
c  71)          "                      80%
c  72)          "                      95%
c  73)          "                      99%

c  Language: FORTRAN 90

c  Parameters:
c    abextn:          absorption coefficient (km-1)
c    angs:            angles at which the phase function was computed (degrees)
```

```
c    ans:            input determinor for p_switch
c    asymm:          precomputed asymmetry factor
c    begin_line:     index of beginning angle in num_lines do loop
c    concentration:  concentration of aerosol (g/m**3)
c    deg2rad:        conversion factor
c    density:        number density of aerosol (particles/cc)
c    extn:           extinction coefficient (km-1)
c    end_line:       index of ending angle in num_lines do loop
c    file_name:      input pfn file name
c    g:              computed asymmetry factor
c    id:             internal identification number of pfn file
c    id_check:       numeric portion of pfn file name
c    num_angs:       number of angles/values for pfn
c    num_angs_max    maximum number of angles/values for pfn
c    num_lines:      number of complete lines -2 required to print out angles
c    num_waves:      number of wavelengths contained in pfn file
c    p_switch:       angle and phase function print switch
c    pfn:            phase function value at related angle
c    pfnint:         integral of phase function
c    pi:             PI
c    rh:             relative humidity (%)
c    scextn:         scattering coefficient (km-1)
c    ssa:            single scattering albedo
c    uin:            input unit number
c    udat:           unit number assigned to phase function file
c    uout:           output unit number
c    version:        indicator for pfn database version
c    w_switch:       no valid wavelength indicator
c    wave:           wavelength (micrometers)
c    wavein:         selected wavelength to print (0 == all)

c  References:
c    Shirkey, R.C., and D.H. Tofsted, "High Resolution Electro-Optical Aerosol
c    Phase Function DataBase, PFNDAT2006", ARL-TR-3877, August 2006, WSMR, NM.
c
c    Shirkey, R.C., and D.H. Tofsted, "Electro-Optical Aerosol Phase Function
c    Database, PFNDAT2005", ARL-TR-3684, November 2005, WSMR, NM.
c
c    Tofsted, D., B. Davis, A. Wetmore, J. Fitzgerrel, R. Shirkey,
c    B. Sutherland, "EOSAEL92 Aerosol Phase Function Data Base PFNDAT,"
c    ARL-TR-273-9, June 1997, WSMR, NM.
c
c    Shirkey, R.C., Sutherland, R.A. and M.A. Seagraves, EOSAEL 87, v26,
c    "Aerosol Phase Function Data Base PFNDAT", ASL-TR-0221-26, October 1987,
c    WSMR, NM.
```

```
  integer, parameter :: num_angs_max = 153            ! 153 angles maximum
  integer :: p_switch, w_switch, uin = 5, uout = 6, udat = 9,
+          begin_line, end_line
  real, dimension(num_angs_max) :: angs, pfn
  real :: wavein, wave, ssa, extn, asymm, scextn
  character (len=9) :: file_name
  character(len=1) ans

  w_switch = 0
  p_switch = 0

  write (uout,*) 'Input wavelength of interest (zero for all) '
  read (uin,*) wavein
  write (uout,*)'Do you want the phase function printed out? (Y/N) '
  read (uin,*) ans
  if (ans == 'Y' .or. ans == 'y') p_switch = 1
  write (uout,*) 'Input file name '
  read (uin,*) file_name                          ! name of pfn file to be examined

  open (udat,file_name,status='old',err=20)

  read (udat,*) version                           ! 87 & 92 will have zero as first value
  rewind (udat)                                   ! 2005/6 has ID first value
  write(uout,*) ' '

  if (version > 0.0) then
     write(uout,'(1x,6x,"  ****** Results for PFNDAT 2005/6 ",a6,
+              " ******")') file_name
     read (udat,*) id,num_angs,num_waves,concentration,density,rh
  else
     write(uout,'(1x,6x,"   ****** Results for PFNDAT 87/92 ",a6,
+              " ******")') file_name
     num_waves = 32                               ! 32 wavelengths/file max
     num_angs = 65
  endif
  write (uout,*) ' '
  write (uout,*) 'For file ',file_name
  write (uout,*) ' '

  read (udat,*) (angs(i),i=1,num_angs)
  do j = 1, num_waves                             ! # of wavelengths in a given file
    if (version > 0.0) then                       ! 2005/6
      read (udat,*,end=30) wave, ssa, extn, asymm    ! different number of wavelengths
                                                     ! in different versions of PFNDAT
      scextn = ssa * extn
```

```
      else                                  ! 87 or 92
        read (udat,*,end=30) nang,id,wave,ssa,extn,scextn
      endif
      read (udat,*,end=31) (pfn(i),i=1,num_angs)
31    abextn = extn - scextn
      if (p_switch == 1 .and. (wave==wavein .or. wavein==0.0)) then
        write (uout,*) 'Angles follow'
        write (uout,'(1x,11(1x,f6.3))') (angs(i),i=1 ,11)
        write (uout,'(1x,11(1x,f6.3))') (angs(i),i=12,22)
        num_lines = (num_angs - 22) / 11
        begin_line = 23
        do k = 1,num_lines
         end_line = begin_line + 10
         write (uout,'(1x,11(f6.2,1x))')
     +                    (angs(i),i=begin_line,end_line)
         begin_line = begin_line + 11
        enddo
        write (uout,'(1x,10(f6.2,1x))')
     +                    (angs(i),i=begin_line,num_angs)
        write (uout,*) ' '
        write(uout,*) 'Phase function follows for wavelength = ',
     +              wave,' um'
        do k = 1, num_angs,6
          if (k+5 < num_angs) then
            write (uout,'(1x,6(E12.6,1X))') (pfn(i),i=k,k+5)

          else
            kn = k+2
            if (num_angs == 65) kn = k+4
            write (uout,'(1x,6(E12.6,1X))') (pfn(i),i=k,kn)

          endif
        end do
        write (uout,*) ' '
      endif                                 ! end optional print

      call integrator(pfn,angs,pfnint,g,num_angs)

      if (wave == wavein .or. wavein == 0.0) then
        w_switch = 1
        write(uout,*) 'Associated information for ',file_name,
     +              ' at wavelength = ',wave,' um'
        write (uout,*) ' Single scattering albedo   = ',ssa
        write (uout,*) ' Coefficients (km-1)'
        write (uout,*) '     extinction = ',extn
        write (uout,*) '     scattering = ',scextn
```

```
          write (uout,*) '     absorpton  = ',abextn
          if (version > 0.0) then
            write (uout,*) ' Asymmetry               = ',asymm  ! 2005/6 precalculated
          else
            write (uout,*) ' Asymmetry               = ',g      ! on-the-fly; 87 & 92
          endif
          write (uout,*) ' Integral of phase function = ',pfnint
          if (version > 0.0) then                          ! additional info for 2005/6
            write (uout,*) ' Relative humidity         = ',rh,' %'
            write (uout,*) ' Concentration             = ',
     +                              concentration,' g/m**3'
            write (uout,*) ' Density                   = ',density,
     +                                    ' particles/cc'
          endif
        write (uout,*) ' '
        write (uout,*) ' '
        endif

      end do                                          ! wavlength loop
30    close (udat)
      if (w_switch == 0) write (uout,*) 'The input wavelength value of '
     +                          ,wavein,' is invalid'
      stop

20    write(uout,*) ' File ',file_name,' does not exist'

      end

      subroutine integrator (pfn,angs,pfnint,g,num_angs)
      real, dimension(num_angs) :: angs, pfn                ! 65/153 angles max
      real(kind=8) :: deg2rad, pi

      pi = 3.1415926535
      deg2rad = pi/180.

c calculate normalization and asymmetry of phase function
      pfnint = 0.0
      g = 0.0

      do i = 1,num_angs - 1                                 ! over zenith angle theta
        pfnint = pfnint + .5*(pfn(i) + pfn(i+1))*           ! zero to pi or zero to 180
     1          abs(dcos(dble(angs(i+1))*deg2rad)-
     2              dcos(dble(angs(i))*deg2rad))

        g = g + .5*(dcos(dble(angs(i))*deg2rad)*pfn(i)+
     1          dcos(dble(angs(i+1))*deg2rad)*pfn(i+1))*
```

```
2          abs(dcos(dble(angs(i+1))*deg2rad)-
3             dcos(dble(angs(i))*deg2rad))
 end do

 pfnint = 2.* pi * pfnint                          ! over azimuthal angle phi
 g = 2. * pi * g / pfnint                          ! zero to 2*pi or zero to 360

 return
 end
```

Acronyms and Abbreviations

AMP	air mass parameter
ARL	U.S. Army Research Laboratory
CL	concentration length
HC	hexachloroethane
HG	Henyey-Greenstein
HE	high explosive
IR	infrared
LOS	line of sight
MBL	marine boundary layer
MG	modified gamma
MMD	mass median diameter
NAM	Navy Aerosol Model
OPAC	Optical Properties of Aerosols and Clouds
PFNDAT	Phase Function Database
RH	relative humidity
T	transmission
TAWS	Target Acquisition Weapons Software
WP	white phosphorus
ZnCl2	zinc chloride

Distribution List

Distribution	Copies
Army Research Laboratory Attn: AMSRD-ARL-D 2800 Powder Mill Road Adelphi, MD 20783-1197	1
Army Research Laboratory Attn: AMSRD-ARL-RO-EN (Dr. Bach) PO Box 12211 Research Triangle Park, NC 27009	1
Army Research Laboratory Attn: AMSRD-ARL-CI-EE (Dr. Shirkey) WSMR, NM 88002-5501	4
Army Research Laboratory Attn: AMSRD-ARL-CI-EE (Dr. O'Brien) WSMR, NM 88002-5501	1
Army Research Laboratory Attn: AMSRD-ARL-CI-EE (D. Tofsted) WSMR, NM 88002-5501	4
Army Research Laboratory Attn: AMSRD-ARL-CI-EE (D. Hoock) APG, MD 21005-5067	1
~~Army Research Laboratory~~ ~~Attn: AMSRD-ARL-SL-BB (R. Sandmeyer)~~ ~~APG, MD 21005~~	~~1~~
Army Materiel Systems Analysis Activity Attn: AMXSY-SC (J. Mazz) 392 Hopkins Road APG, MD 21005-5071	1
US Army Night Vision & Electronic Sensors Directorate Performance Model Development Branch Attn: AMSRD-CER-NV-MS-PMD (J. Hixson) 10221 Burbeck Road Fort Belvoir, VA 22060-5806	1
Army Modeling & Simulation Office DA G37 (DAMO-SBM) 400 Army Pentagon Washington, DC 20310-0450	1
Director, USA TRADOC Analysis Center Attn: ATRC-W (P. Blechinger) WSMR, NM 88002-5502	1
Director, USA TRADOC Analysis Center Attn: ATRC-WA (L. Southard) WSMR, NM 88002-5502	1
ERDC/CRREL Attn: Dr. G. Koenig 72 Lyme Rd Hanover, NH. 03755	1
Army Corps of Engineers Topographic Eengineering Center Data and Signature Analysis Branch Ft. Belvoir, VA 22060	1
US Military Academy Dept of Mathematical Sciences Thayer Hall West Point, NY 10996-1786	1
United States Military Academy Combat Simulation Laboratory (Dr. P. West) West Point, NY 10996	2
~~USA PEO STRI~~ ~~FCS Training IPT Environment~~ ~~D. Stevens~~ ~~12350 Research Pkwy~~ ~~Orlando, FL 32826-3276~~	~~1~~
AFRL/IFOIL 525 Brooks Road Rome, NY 13441-4505	1
Air Weather Service 151 Patterson Ave Rm. 120 Asheville, NC 28801-5002	1
HQ USAFA/DFLIB 2354 Fairchild Drive, Suite 3A10 USAF Academy, CO 80840-6214	1

Distribution	Copies
Tech Connect AFRL/XPTC Bldg 16, Rm 107 2275 D Street WPAFB, OH 45433-7226	1
Dr. Andy Goroch Naval Research Laboratory Marine Meteorology Division, Code 7543 7 Grace Hopper Ave Monterey, CA 93943-5006	1
U.S. Naval War College War Gaming Department (Code 33) 686 Cushing Road Newport, Rhode Island 02841-1207	1
Naval Postgraduate School J. D. Eagle OR/Er 1 University Circle Monterey, CA 93943	1
Naval Postgraduate School R. K. Wood OR/Wd 1 University Circle Monterey, CA 93943	1
Naval Postgraduate School G. Schacher Dept. of Physics 1 University Circle Monterey, CA 93943	1
Naval Postgraduate School W. B. Maier II Dept. of Physics 1 University Circle Monterey, CA 93943	1
Ruth H. Hooker Research Library 4555 Overlook Ave, SW Washington, DC 20375	1
JWARS Attn: C. Burdick 1555 Wilson Boulevard, Suite 619 Arlington, VA 22209	1
U.S. Army Research Laboratory AMSRD CI OK TP Techl Lib APG, MD 21005	2
Northrop Grumman Attn: Info Tech M. Gouveia 55 Walkers Brook Dr. Reading, MA 01867	1
Northrop Grumman Information Technology Dr. Haig Iskenderian 55 Walkers Brook Dr. Reading, MA 01867	1
Anteon Corp. Mike Adams 46 Growing Rd Hudson, NH 03051	1
SAIC Attn: Mr. Delgado 731 Lakepointe Centre Dr. O'Fallon, Ill 62269-3064	1
Technical Reports Boulder Laboratories Library, MC 5 325 Broadway Boulder, CO 80305	1
NCAR Library Serials National Center for Atmospheric Research PO Box 3000 Boulder, CO 80307-3000	1
U.S. Army Research Laboratory Attn: IMNE ALC IMS Mail & Records Mgmt Adelphi, MD 20783-1197	1
Admnstr Defns Techl Info Ctr Attn: DTIC OCP (V Maddox) 8725 John J Kingman Rd., Ste. 0944 Ft Belvoir, VA 22060-6218	1 elec
U.S. Army Research Laboratory AMSRD ARL CI OK TL Techl Lib 2800 Powder Mill Rd. Adelphi, MD 20783-1197	2
Dr. R. Rasmussen National Center for Atmospheric Research P.O. Box 3000 Boulder, CO 80307-3000	1
TOTAL	50

INTENTIONALLY LEFT BLANK